AD-A092 987 PARIS-6 UNIV (FRANCE) LABORATOIRE DE PHYSIQUE DES SOLIDES F/G 7/4
DEFECTS AND DISORDER PRODUCED BY ION IMPLANTATION IN SOLIDS.(U)
SEP 80 J F MORPANGE, G KANELLIS, M BALKANSKI DA-ERO-78-G-002

UNCLASSIFIED NL

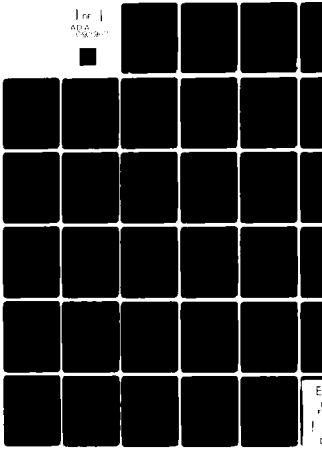

END
DATE FILMED
1-81
DTIC

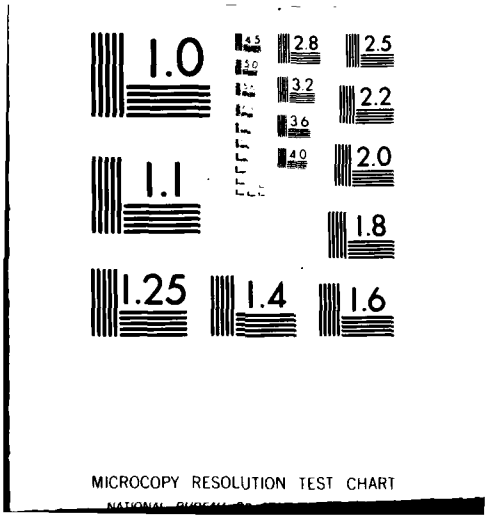
1.0
1.1
1.25
1.4
1.6
1.8
2.0
2.2
2.5
2.8
3.2
3.6
4.0
MICROCOPY RESOLUTION TEST CHART

# DEFECTS AND DISORDER PRODUCED BY ION IMPLANTATION IN SOLIDS

Final Report

by

J.F. MORHANGE
G. KANELLIS
and M. BALKANSKI

September 1980

EUROPEAN RESEARCH OFFICE
United State Army
London - England



GRANT NUMBER DA-ERO 78-G-002
Université Pierre et Marie Curie
Paris, France

UNCLASSIFIED

SECURITY CLASSIFICATION OF THIS PAGE (When Data Entered)

R&D 2381

# REPORT DOCUMENTATION PAGE

READ INSTRUCTIONS BEFORE COMPLETING FORM

| | |
|---|---|
| 1. REPORT NUMBER | 2. GOVT ACCESSION NO. AD-A092 987 |
| 3. RECIPIENT'S CATALOG NUMBER (9) | |
| 4. TITLE (and Subtitle) Defects and Disorder Produced by Ion Implantation in Solids. | 5. TYPE OF REPORT & PERIOD COVERED Final Technical Report, Oct 77 – Oct 80 |
| | 6. PERFORMING ORG. REPORT NUMBER |
| 7. AUTHOR(s) J.F./Morhange M./Balkanski G./Kanellis (1) (15) | 8. CONTRACT OR GRANT NUMBER(s) DAERO-78-G-002 |
| 9. PERFORMING ORGANIZATION NAME AND ADDRESS Universite Pierre et Marie Curie Paris, France | 10. PROGRAM ELEMENT, PROJECT, TASK AREA & WORK UNIT NUMBERS 61102A1T161102BH57-03 (16) (17) |
| 11. CONTROLLING OFFICE NAME AND ADDRESS USARDSG-UK Box 65, FPO NY 09510 (11) | 12. REPORT DATE September 1980 |
| | 13. NUMBER OF PAGES 64 |
| 14. MONITORING AGENCY NAME & ADDRESS(if different from Controlling Office) | 15. SECURITY CLASS. (of this report) Unclassified |
| | 15a. DECLASSIFICATION/DOWNGRADING SCHEDULE |

16. DISTRIBUTION STATEMENT (of this Report)

Approved for Public Release; Distribution Unlimited

17. DISTRIBUTION STATEMENT (of the abstract entered in Block 20, if different from Report)

18. SUPPLEMENTARY NOTES

19. KEY WORDS (Continue on reverse side if necessary and identify by block number)

Ion implantation; Annealing; Laser annealing; Gallium arsenide; Silicon; Optical properties; Raman spectroscopy

20. ABSTRACT (Continue on reverse side if necessary and identify by block number)

Silicon and Gallium Arsenide samples doped by ionic implantation have been characterized by Raman spectroscopy. A specific behaviour under laser annealing has been shown. This behaviour can be explained by the presence of microcrystallites in the annealed region. A model describing vibrational properties of the microcrystallites has been established and compared with experimental results.

DD FORM 1 JAN 73 1473 EDITION OF 1 NOV 65 IS OBSOLETE

UNCLASSIFIED

SECURITY CLASSIFICATION OF THIS PAGE (When Data Entered)

## ABSTRACT

Silicon and Gallium Arsenide samples doped by ionic implantation have been characterized by Raman spectroscopy. A specific behaviour under laser annealing has been shown. This behaviour can be explained by the presence of microcrystallites in the annealed region. A model describing vibrational properties of the microcrystallites has been established and compared with experimental results.

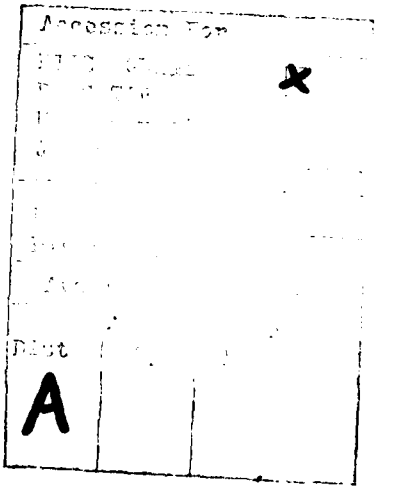

# TABLE OF CONTENTS

## LIST OF ILLUSTRATIONS

# 1. INTRODUCTION

The increasing technological qualities required for the realization of microelectronic devices need a better contr l of the doping process. The ion implantation appears to be an answer to this demand by allowing a fine control of the doping profile. However, the radiation damages induced by the ion beam have to be annealed in order to recover crystalline and electrical properties. Raman spectroscopy which is non destructive probes the vibrational properties of the material and is well suited to test the implantation effects and the annealing behaviour in Gallium Arsenide. The thermal annealing behaviour has yet been studied and results have been exposed in the First Technical Report DA-ERO 78-G-002 (March 1979) and will only be summarized here.

As thermal annealing is time consuming and can destroy the doping profile by diffusion of the dopants, the microelectronic industry is now testing a new method of annealing using high power pulsed laser. This new annealing technique presents an interest as well for the technological applications as for fundamental research. In fact, up to now the laser annealing process is controversed. Two different processes have been proposed in the literature . The first one, the older,implies a pure thermodynamic effect (melting of the material), the second one proposes an electric field effect (generation of a high density plasma of free carriers). The Raman spectroscopy can characterize the effect of laser annealing and the results which are presented here show completely different spectra as compared to the spectra of classical thermal annealed samples. To justify those results we have been lead to compute the vibrational mode frequencies of a truncated crystal. Although a crude reduction is made in order to compute the frequencies of the modes, the comparison between the Raman spectra and the theoretical results is satisfying.

## 2. THERMAL ANNEALING

The results obtained are just summarized here as they have been developped in the First Technical Report (March 1979).

The stability of the substrate (semi insulator GaAs) has been first tested as GaAs is well known to be unstable at high temperature. For low temperature annealing (under 500° C) no sensible modification can be observed on the two first order Raman peaks allowed in GaAs. Above 500° C the quality of the surface is degraded and the selection rules are partially modified. A weak peak is observed for geometries where it is normally forbidden. The protection effect of a $Si_3N_4$ protective coating has been evidenced, the forbidden peak being smaller in this case.

The annealing kinetics have thus been studied at temperature much lower than 500° C in order to avoid stability problem. Isothermal and isochronal annealing have been studied with specific interest for isochronal ones which allow the determination of the recrystallization velocity. The electrical activity after the annealing of a GaAs sample implanted with Sulphur has been measured using the coupling phonon LO-plasmon. This measure is rather imprecise and gives essentially the concentration of free carriers at the maximum of the implantation profile. No impurity modes (localized modes) could be detected due to the low solubility limit of dopants in GaAs and the low sensibility of Raman spectroscopy to this effect.

## 3. LASER ANNEALING

The recovery of crystalline and electrical properties of implanted samples needs an annealing which is time consuming and which can flatten the steep doping profile by diffusion of the doping ions, destroying one of the best advantages of ionic implantation over classical techniques. Recently, a new method of annealing disordered material has been introduced : the pulsed laser irradiation[1, 2, 3]. Semiconductors are subjected to high energy irradiation using Q switch laser (Ruby or YAG with frequency doubler). The advantages of this technique are obvious on the time of processing, and there exists the possibility of focussing the laser spot to achieve very local treatment.

The reordering process is,up to now,not clearly understood. At the present time two different processes are proposed. The older one is supported by time resolved reflectivity experiments during the pulse[4]. It supposes that the effect of the irradiation is only a thermal one. The material is fused and the recrystallization occurs through a liquid epitaxial process if the fused region reaches the crystalline to amorphous substrate, the material becoming monocrystalline. If the fused region does not reach the interface, recrystallization occurs through some kind of nucleation process,the material becoming,in that case, polycrystalline.

A more recent theory[5, 6] takes in account the effect of the electric field of the annealing laser,which creates a dense plasma of free carriers. This theory is supported by a Raman experiment during the pulse[7].

The results presented here cannot decide between the two processes the Raman spectra being taken on yet annealed samples after the pulse, but they can characterize the quality of recrystallization. The first experiments were carried out on Silicon sample, this material being the most widely studied.

## 3.1. Laser annealing on Silicon

The laser used for these experiments was a Ruby laser ($\lambda$ = 694 nm) with pulse duration of 100 ns. The energy density was varied between 0.5 J/cm$^2$ and 3 J/cm$^2$, the value for which severe degradation occured on the surface of the sample. Silicon samples were amorphized by implantation of Silicon ions. The diameter of the spot of the Raman laser is of the order of 80 µm, the diameter of the annealed zone is of the order of 2 mm. This fact allows us to sweep the Raman laser spot onto the surface of the annealed region, realizing a topography of this region.

Two thicknesses of amorphous material have been tested, 150 nm and 500 nm, corresponding respectively to implantation conditions of $2.10^{15}$ at /cm$^2$ at 80 keV or $2.10^{15}$ at /cm$^2$ at 80 keV $\pm$ $2.10^{15}$ at /cm$^2$ at 200 keV $\pm$ $2.10^{15}$ at /cm$^2$ at 300 keV. The wavelength of the Raman laser was the 488 nm of the Argon laser whose penetration depth is of the order of 1000 nm in single crystal, and about 100 nm for amorphous material.

The Figure 1 presents the Raman spectra of the 500 nm thick layer for various points of the annealed zone. At the center of the zone the Raman peak is shifted towards low frequencies from about 1 cm$^{-1}$, its width being doubled (6 cm$^{-1}$). Approaching the periphery, the shift and the broadening of the peak are amplified. The Figure 2 shows the behaviour of the spectra just in the neighbourhood of the periphery of the annealed zone where the amorphous band is still observable. As it can be seen, this amorphous band modes towards higher frequencies until it merges with the phonon peak and remains as a tail on the lower frequency side of this peak.

The next Figure (Figure 3) shows Raman spectra from the 150 nm thickness. At the center of the annealed region one peak appears situated at the true frequency of single crystal. The intensity of this peak decreases while going towards the periphery.

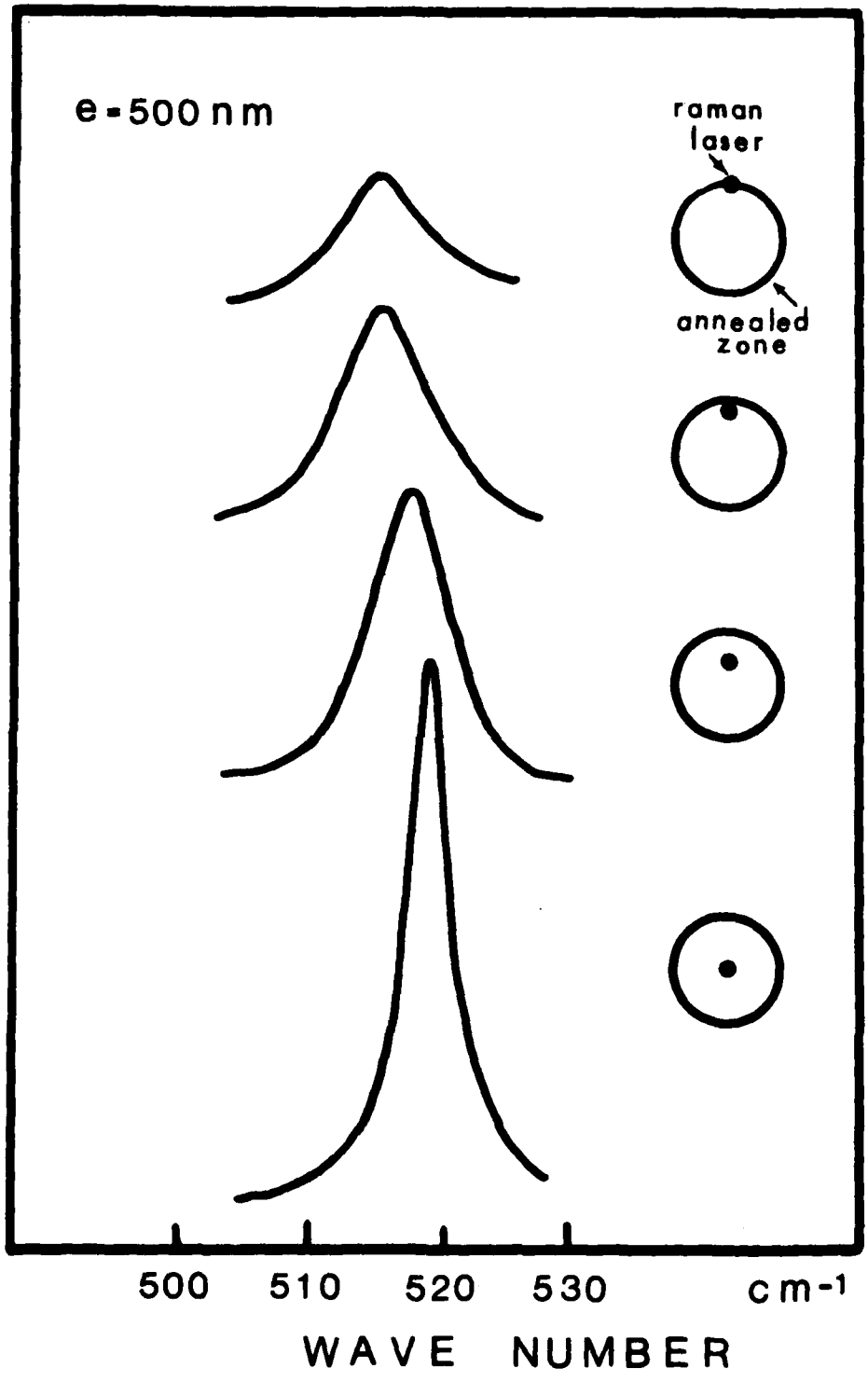


Figure 1. Raman spectra of a laser annealed 500 nm thick amorphous layer of Silicon coming from various points of the sample.

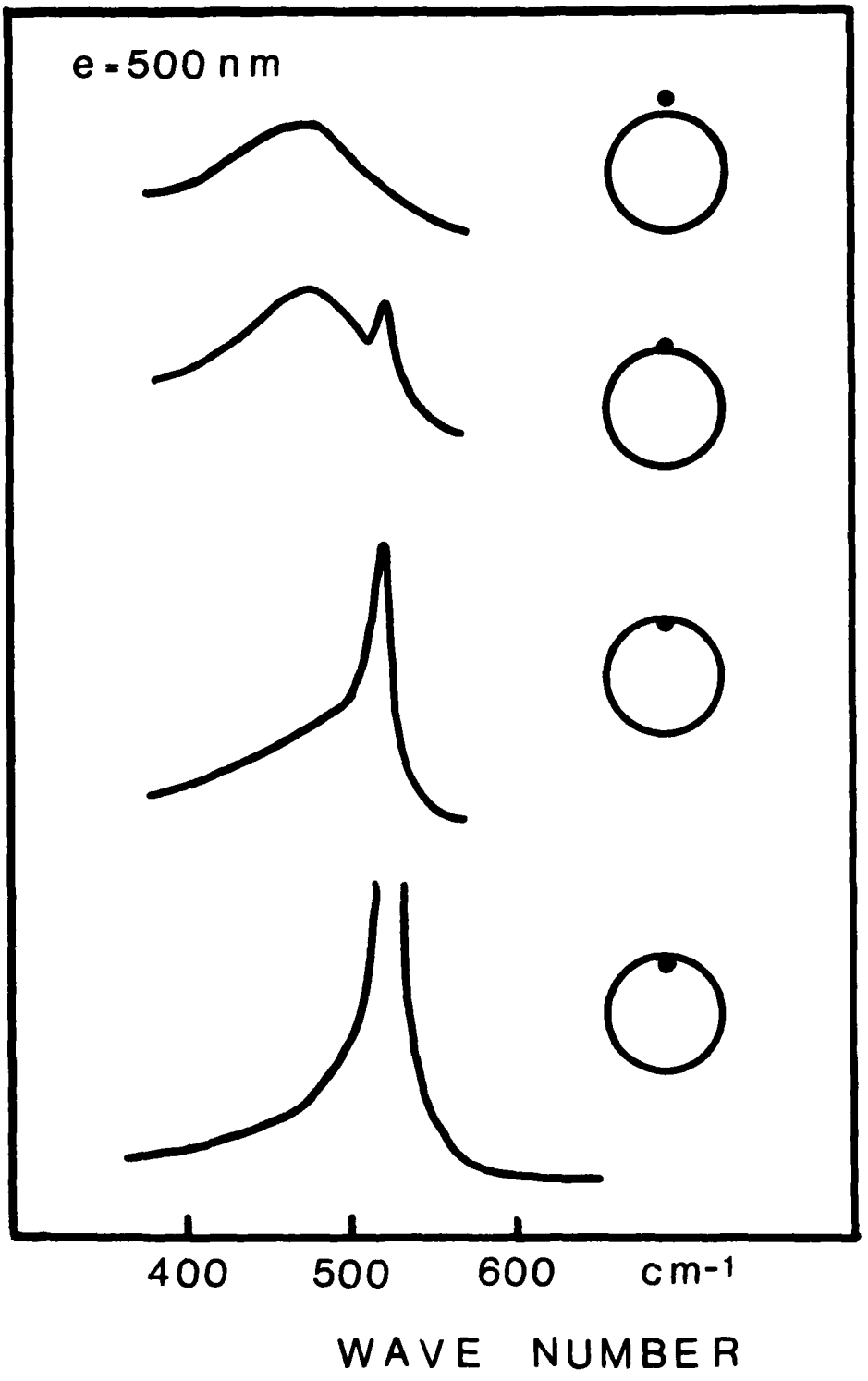


Figure 2. Raman spectra of a laser annealed 500 nm thick amorphous layer near the periphery of the annealed region.

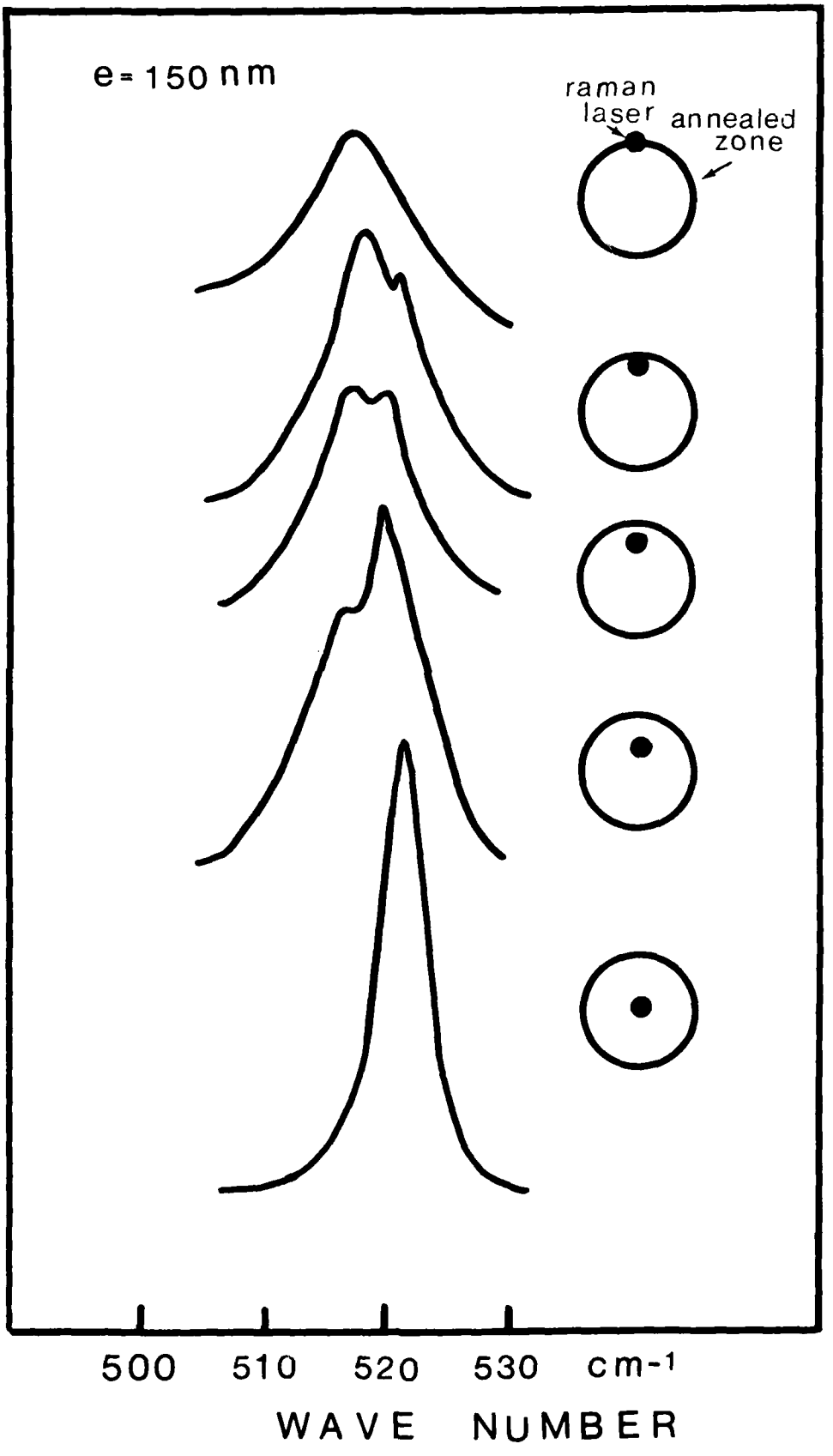


Figure 3. Raman spectra of a laser annealed 150 nm thick amorphous

frequency and the shift reaches 6 $cm^{-1}$ at the edge of the zone.

Such results can be interpreted by supposing the existence of microcrystallites of continuously varying size from the center to the periphery of the annealed region. The frequency shift is thus induced by the new conditions to the limit which modify the force constants. The presence of microcrystallite in the laser annealed samples is not only an hypothesis as they have been observed by transmission electronic microscopy[8].

The difference observed from the different thicknesses can be explained as follow : Without choosing between the two recrystallization processes, it seems reasonable that if the region of the sample modified during the irradiation (melted zone or region of high density plasma) reaches the crystalline-amorphous interface , the material will recrystallize in monocrystalline form. It will recrystallize in polycrystalline form if this region does not reach the interface. For the thin amorphous layer, the interface has been reached at least at the center where the irradiation energy is maximum so that the center of the zone is monocrystalline, which delivers a non shifted Raman peak, whereas for the thicker layer, the interface was not reached, resulting in a polycrystalline material on all the surface of the annealed region. In this last case, the Raman peak is shifted, even at the center of the annealed region.

## 3.2. Laser annealing in GaAs

The same work of characterization has been carried out on Gallium Arsenide samples. These samples (semi insulating) were implanted with $2.10^{14}$ at /$cm^2$ of As and $2.10^{14}$ at /$cm^2$ of Ga under 300 keV. These conditions result in the formation of an amorphous thickness of about 2000 Å. The pulsed laser was YAG laser with frequency doubler (530 nm).

Gallium Arsenide being partially ionic, the degeneracy between LO and TO phonon is split and so two peaks are generally

observed in the Raman spectra.

However, it is possible, by aligning specific crystalline axes of the sample with the direction of the electric field of the incident laser and of the scattered light to extenguish one or both of these two peaks. Working in a backscattering geometry, the TO phonon is extinguished when the face of the sample normal to the light is a (100) face. It is the LO phonon which vanishes for a (110) face. The next Figures (4 and 5) show Raman spectra in these two cases, for various energies of irradiation.

For the (100) face the behaviour is spectacular. At low energy of irradiation, the forbiden peak (TO) is bigger than the allowed one ; as the energy increases, the intensities are inverted and the selection rules are more or less observed for energy irradiation of 0.6 $J/cm^2$. For the (110) face, the forbidden peak (LO) is only weakly activated at low energy and its intensity decreases as the irradiation energy increases. The spectacular results observed on the (100) face have lead us to study more completely the polarization behaviour. This is presented on Figure 6. Irradiation energy was 0.6 $J/cm^2$ and the Raman laser spot was swept onto the surface of the annealed zone in the same manner as for Silicon.

For the electric fields parallel,selection rules allow the LO phonon,whereas for perpendicular fields both phonons are forbidden. This is well observed at the center of the zone,but at the periphery, the peaks are completely depolarized.

This behaviour can be interpreted in the same way as for Silicon by the presence of microcrystallites in the annealed region. The depolarization observed is explained by the misalignment of these crystallites. The very strong occurence of the TO phonon in a geometry where it should be forbidden is a consequence of the limitation (surfaces) of the very little crystallites which restrain the long range electric forces responsible of the longitudinal phonon.

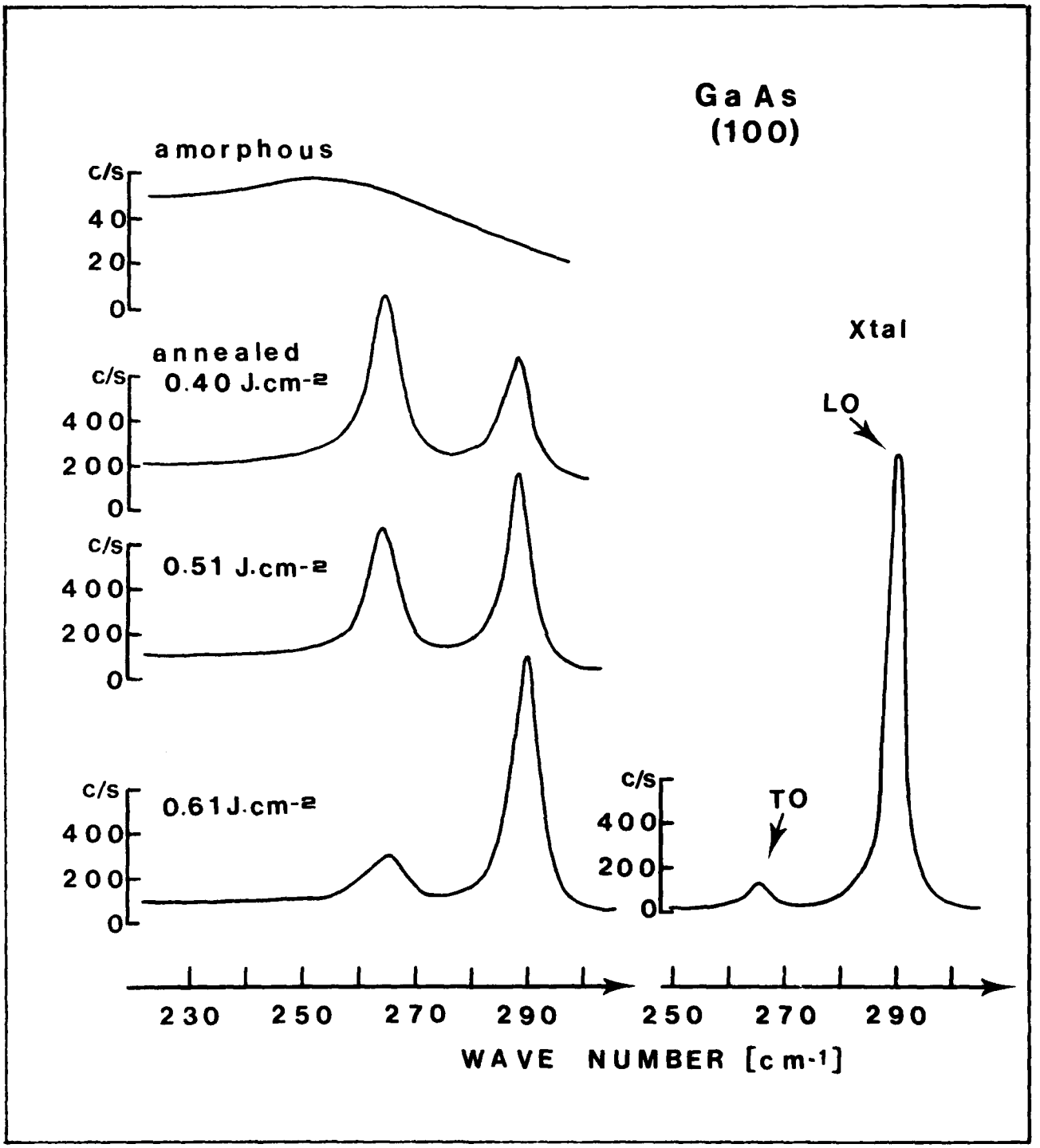


Figure 4. Raman spectra of a laser annealed sample of GaAs (100) for various energy densities.

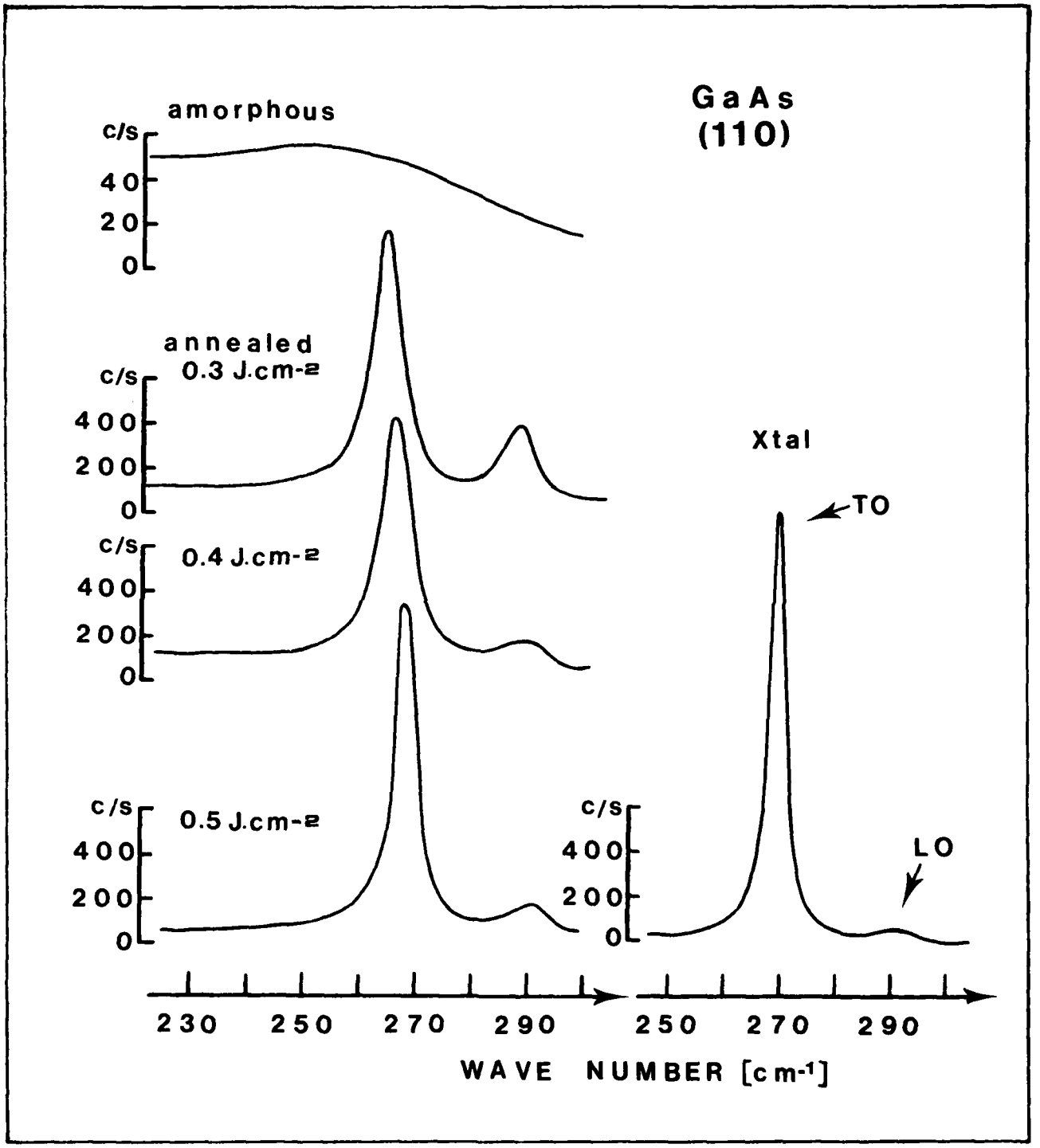


Figure 5. Raman spectra of a laser annealed sample of GaAs (110) for various energy densities.

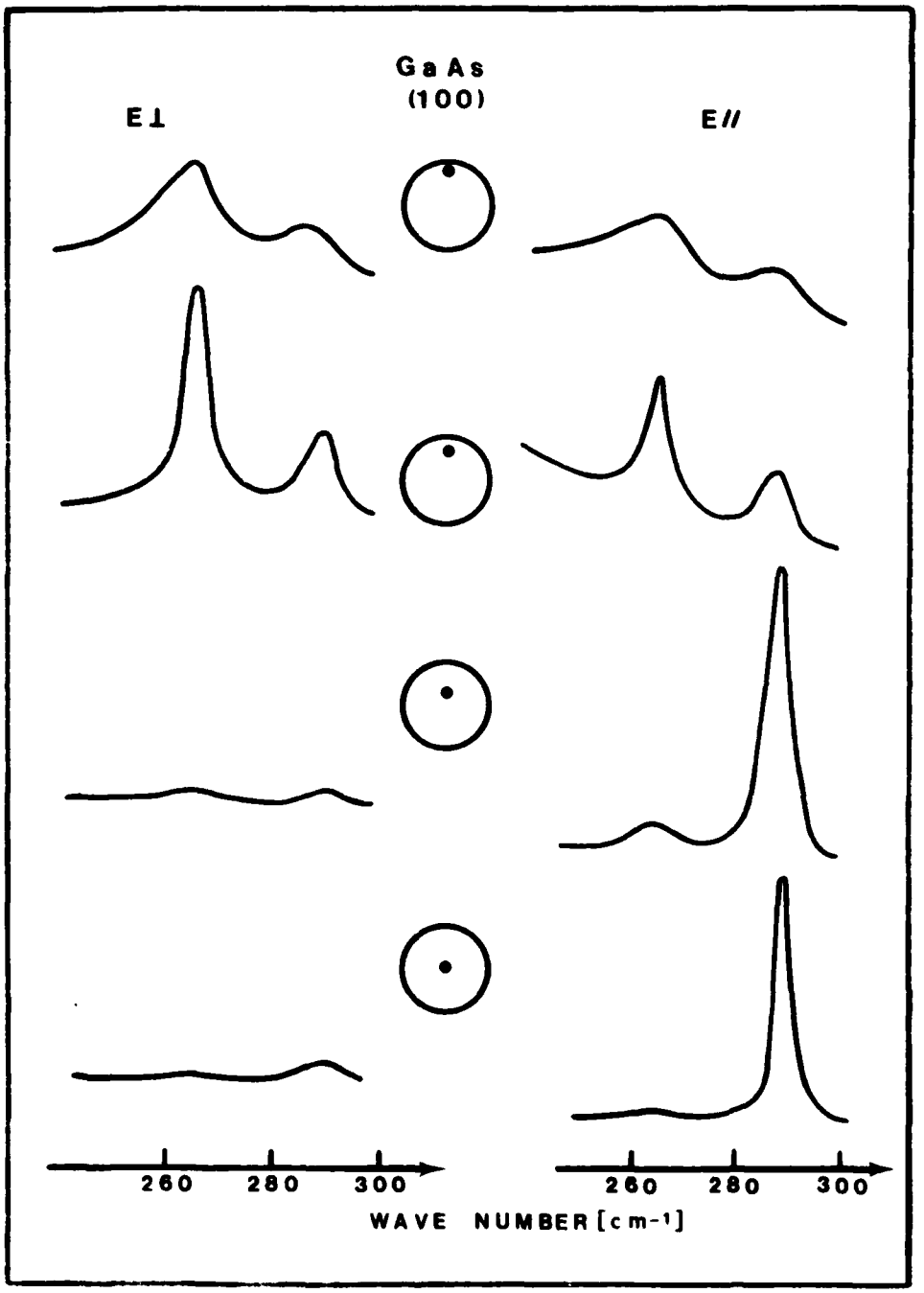


Figure 6. Raman spectra of a laser annealed sample of GaAs (100) from various points of the sample. The incident field is parallel to a 110 axe, the scattered field is perpendicular or parallel to the incident field.

## 4. THEORETICAL MODEL

In order to account for the variation of the frequency of the first order Raman peaks, a calculation of the vibration modes of a microcrystallite must be done. The classical approach of this problem is the diagonalization of the dynamical matrix. As the microcrystallite is by nature limited in size, the usual symmetry of translation is suppressed and then the Born-Van Karman cyclic conditions can no more be applied to reduce the dynamical matrix. Instead of a 3s order matrix in the case of a perfect crystal (s = number of atoms in the unit cell), the dynamical matrix is now of order 3 N (N = total number of atoms) for a limited crystallite. The diagonalization of such a matrix rapidly becomes impossible. For example,a cube of 100 $\mathring{A}^3$ of Silicon contains of the order of 50 000 atoms leading to a 150 000 x 150 000 matrix. Moreover,to achieve the computation,a complete knowledge of the geometric surface structure is necessary. For these reasons, we have choosen a simpler way, the calculation of the frequencies of the vibration modes of a thin layer of material. This slab is extended to infinity in two directions and comprises various number of layers,each of which has the thickness of a unity cell.

In such a structure, the periodicity is conserved along two directions,and consequently the atomic displacement parallel to these directions can be expanded in plane waves and the cyclic conditions can be applied. Along the third direction, neither of the above consideration is possible and,the sequence of cells along that direction is treated merely as one unit cell. For a slab formed by N cells of the 3 dimensional structure, the dynamical matrix is of order 6N. This matrix will present a simpler form if the orientation of the slab is chosen to be across directions of high symmetry. For blende and diamond structure in which crystallize Gallium Arsenide and Silicon, the (111) plane is favourable. In this case,for the blende structure, the slab is composed of alternate layers of anions and cations. These ions are identified by the index pair $(l_3, k)$,where $l_3$

($l_3$ = 1, 2, ... N) numbers the pair of plane and k (k = 1,2) numbers the ions (Figure 7). The symmetry of the bidimensional structure implies that the sub matrix 3 x 3 which describes the interaction between two layers ($l_3$, k) and ($l_3'$, k') are for $\vec{q}$ = 0 of the form

$$D\begin{pmatrix} l_3 , k \\ l_3' , k' \end{pmatrix} = \begin{pmatrix} A & B & -B \\ B & A & -B \\ -B & -B & A \end{pmatrix}$$

which can easily be diagonalized to

$$\begin{pmatrix} A-B & 0 & 0 \\ 0 & A-B & 0 \\ 0 & 0 & A+2B \end{pmatrix}$$

This form implies that the solutions for any slab having the above orientation are separated into two groups, one doubly degenerated containing the solutions corresponding to modes which vibrate parallel to the plane (X-Y modes), and one non-degenerated containing the solutions corresponding to vibrations perpendicular to the surface of the slab (Z modes).

To numerically compute the frequencies of these modes we need now to introduce a model of force constants.

## 4.1. Force constants

The elements of the dynamical matrix can be computed assuming the following considerations :

- The displacement along the axes of the plane are periodic and can be developped in plane wave.

- The potential of interaction is composed of short range forces which act only between the neighbours ions and long range Coulombian forces. This last part of the potential has only to be considered in

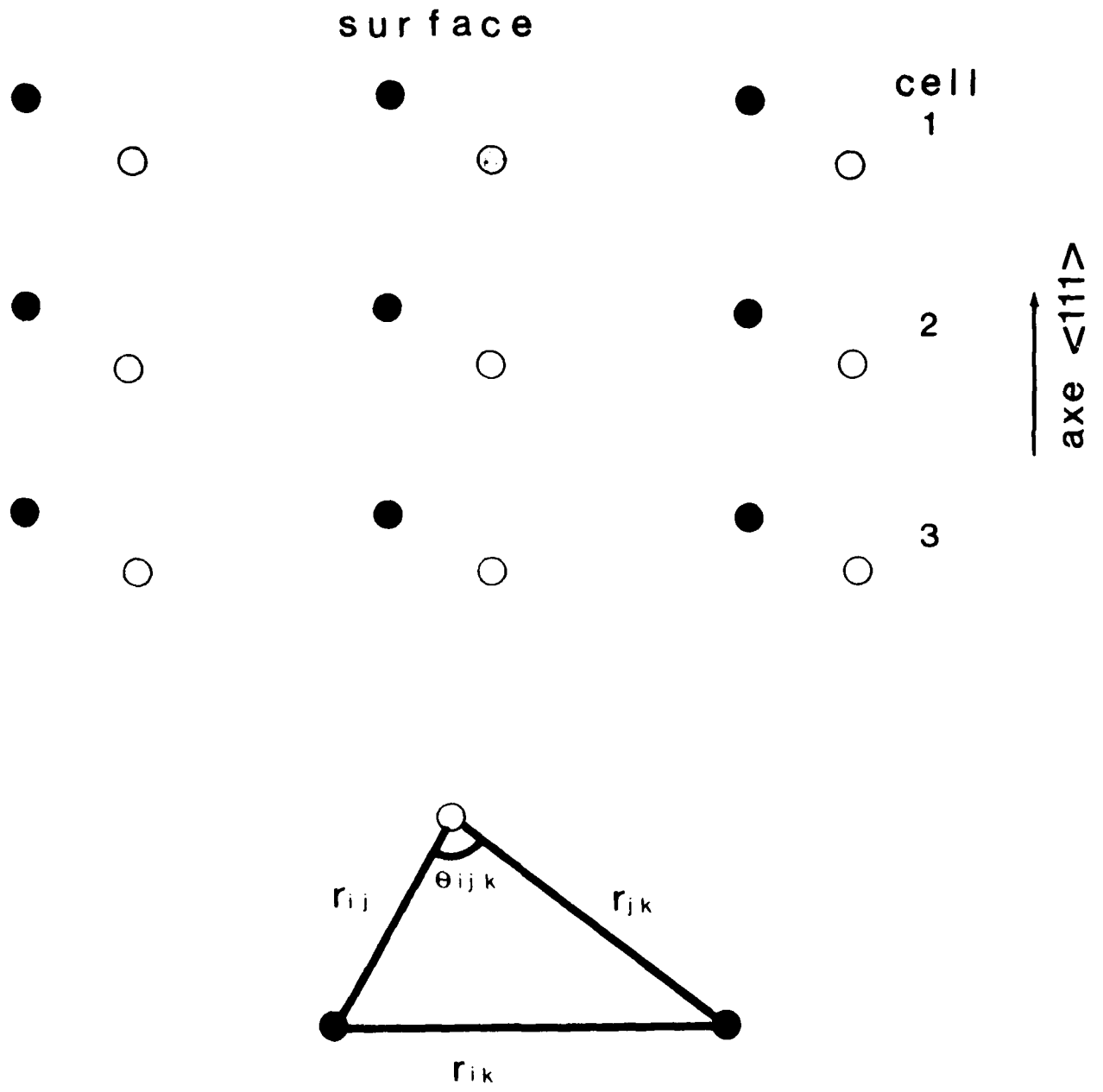


Figure 7. The slab geometry and the forces constants.

ionic crystals like GaAs and not in homopolar crystals like Silicon.

4.1.1. Short range potential

The short range potential is derived from K. Kunc[9]

$$\Delta\phi = r_o\,\xi \sum_{1-2} \Delta r_{ij} + \frac{\lambda}{2} \sum_{1-2} (\Delta r_{ij})^2 + \frac{\sqrt{3}}{4}\,\rho \sum_{2-2} \Delta r_{ik} + \frac{\mu}{2} \sum_{2-2} (\Delta r_{ik})^2 +$$

$$\frac{\sqrt{3}}{4}\,\sigma \sum_{1-1} \Delta r_{jl} + \frac{\nu}{2} \sum_{1-1} (\Delta r_{jl})^2 + \frac{k\theta r_o^2}{2} \sum_{1-2-1} (\Delta\theta_{jil}) +$$

$$\frac{k'\theta\sim o^2}{2} \sum_{2-1-2} (\Delta\theta_{ijk})^2 + \frac{krr}{2} \sum_{1-2-1} \Delta r_{ji}\,\Delta r_{il} + \frac{k'rr}{2} \sum_{1-2-1} \Delta r_{ij}\Delta r_{ik}$$

where $r_o$ is the distance between first neighbours; $\xi$ and $\lambda$ are axial force constants between first neighbours; $\rho$, $\mu$, $\sigma$, $\nu$ are force constants between second neighbours; $K_\theta$, $K_{\theta'}$, $K_{rr}$, $K'_{rr}$ are angular force constant between first and second neighbours; 1 describes the cation and 2 the anion.

The sub matrices of interaction between the planes are different according to the position of the planes (at the surface or inside the volume).

The following cases apply :

1) Interaction between the plane of anions and the plane of cations at the surface of the slab.

$$\begin{pmatrix} 2A_1+A_2 & -B_2 & B_2 \\ -B_2 & 2A_1+A_2 & B_2 \\ B_2 & B_2 & 2A_1+A_2 \end{pmatrix}$$

2) Interaction between a plane of cation and a plane of anion, first neighbours inside the crystal :

$$\begin{pmatrix} 3A & -B & B \\ -B & 3A & B \\ B & B & 3A \end{pmatrix}$$

3) Interaction between a plane of anions and the plane of cations of the next layer inside the crystal :

$$\begin{pmatrix} A & B & -B \\ B & A & -B \\ B & -B & A \end{pmatrix}$$

4) Interaction between the plane of cations and the next plane of cations :

$$\begin{pmatrix} 2C_1+F_1 & D_1 & -D_1 \\ D_1 & 2C_1+F_1 & -D_1 \\ -D_1 & -D_1 & 2C_1+F_1 \end{pmatrix}$$

5) Interaction between the plane of anion and the next plane of anions :

$$\begin{pmatrix} 2C_2+F_2 & D_2 & -D_2 \\ D_2 & 2C_2+F_2 & -D_2 \\ -D_2 & -D_2 & 2C_2+F_2 \end{pmatrix}$$

6) Interaction between the plane of the cations of the first layer inside the volume and the plane of anion at the surface :

$$\begin{pmatrix} 2A_3+A_4 & -B_4 & B_4 \\ -B_4 & 2A_3+A_4 & B_4 \\ B_4 & B_4 & 2A_3+A_4 \end{pmatrix}$$

The coefficients $A_1$, $A_2$, $B_2$, A, B, $C_1$, $D_1$, $F_1$, $C_2$, $A_2$, $F_2$, $A_3$, $A_4$, $B_4$ can be expressed in terms of the force constant as follows:

$$A_1 = -\frac{1}{3}(\lambda + 2\xi) - \frac{4}{3}(k_\theta + k'_\theta) + \frac{1}{6}k'_{rr}$$

$$A_2 = -\frac{1}{3}(\lambda + 2\xi) - \frac{4}{3}k'_\theta + \frac{1}{6}(2k_{rr} + k'_{rr})$$

$$B_2 = -\frac{1}{3}(\lambda + \xi) - \frac{2}{3}k'_\theta + \frac{1}{6}(2k_{rr} + k'_{rr})$$

$$A = -\frac{1}{3}(\lambda + 2\xi) - \frac{4}{3}(k_\theta + k'_\theta) + \frac{1}{6}(k_{rr} + k'_{rr})$$

$$B = -\frac{1}{3}(\lambda + 2\xi) + \frac{2}{3}(k_\theta + k'_\theta) + \frac{1}{6}(k_{rr} + k'_{rr})$$

$$C_1 = -\frac{1}{2}(\rho + \mu) - \frac{1}{6}(k'_\theta + k'_{rr})$$

$$D_1 = \frac{1}{2}(\rho - \mu) - \frac{1}{6}(k'_\theta + k'_{rr})$$

$$F_1 = -\rho - \frac{1}{6}(4k'_\theta + k'_{rr})$$

$$C_2 = -\frac{1}{2}(\sigma + \nu) - \frac{1}{6}(k_\theta + k'_{rr})$$

$$D_2 = \frac{1}{2}(\sigma - \nu) - \frac{1}{6}(k_\theta + k'_{rr})$$

$$F_2 = -\sigma + \frac{1}{6}(4k_\theta + k'_{rr})$$

$$A_3 = -\frac{1}{3}(\lambda + 2\xi) - \frac{4}{3}(k_\theta + k'_\theta) + \frac{1}{6}k'_{rr}$$

$$A_4 = -\frac{1}{3}(\lambda + 2\xi) - \frac{4}{3}k_\theta + \frac{1}{6}(k_{rr} + k'_{rr})$$

$$B_4 = -\frac{1}{3}(\lambda - \xi) + \frac{2}{3}k_\theta + \frac{1}{6}(k_{rr} + 2k'_{rr})$$

### 4.1.2. Long range potential

For ionic crystals, the Coulombian electric forces must be added to the short range forces. These long range forces are theoretically computed, using the formula :

$$\sum_{\beta} \frac{\partial^2}{\partial X_\alpha \partial X_\beta} \sum_{1} \frac{\exp\,(2\pi i\, \vec{Y}.\vec{X}_{(1)})}{|\vec{X}_{(1)} - \vec{X}|}$$

The calculation of expressions of this sort implies slowly convergent sums and diverging terms. Up to now we have not yet succeeded in including this long range potential in our model, so that we will only present here results on homopolar crystals, for which only short range potential applies.

## 4.2. Force constants for Silicon

In the case of Silicon, the higher symmetry of the diamond structure, as compared to the blende one, involves some reduction, as both atoms of the unit cell are identical. The following coupling parameters: $\rho$, $\mu$, $k_\theta$, $k_{rr}$ are now respectively equal to $\sigma$, $\nu$, $k'_\theta$, $k'_{rr}$.

Knowing that this model of a thin layer can only give a rough idea of the behaviour of the frequency, a further reduction which neglects the 2nd neighbours interaction seems reasonable. The potential can now be written as :

$$r_o \sum_{1-2} \xi \Sigma \Delta r_{i_j} + \frac{\lambda}{2} \sum_{1-2} (\Delta r_{i_j})^2 + r_o^2\, k_\theta \sum_{1-2-1} (\Delta\theta_{i_{jk}})^2$$

The first sum is null as $\xi$ can be expressed as :

$$-\frac{1}{4}\,\alpha_M \frac{(Ze)^2}{r_o^3} - 4\,(\rho + \sigma)$$

and $\rho$, $\sigma$ have been neglected and $\alpha_M$ is zero for a homopolar crystal. The second sum extends over all first nearest neighbours and the third one over all angles of bonds for each atom .

The potential is now reduced to a simple two constant equation. These constants can be determined by fitting the frequencies of transverse optical modes for three points of the Brillouin zone. The results are summarized in the following table :

| Point in the B2 | Experiment $cm^{-1}$ | calculated $cm^{-1}$ |
|---|---|---|
| TO ($\Gamma$) | 520 | 520 |
| TO (L) | 491 | 491.5 |
| TO (X) | 462 | 461.3 |
| X = 1.296 dyn/Å | - | k = 0.00783 dyn/Å |

The experimental frequencies of the phonons are taken from second order Raman spectra of crystalline Silicon[10].

## 4.3. Results and discussion

The frequencies of vibrational modes for slabs having thickness from 1 to 50 unit cells are calculated. The frequency variation of the higher modes for in-plane and out-of-plane vibrations have been plotted versus the thickness of the slab on Figure 8. These modes should tend to the $\Gamma$ point optical frequency in the limit of the infinite crystal and are thus to compare with the experimental shifted frequency observed in laser annealed Silicon. As can be observed, the frequencies of these two modes shift towards the lower frequency region as observed in the Raman spectra of laser annealed samples,and this result,which was not obvious,is perhaps the most important outcome which can be drawn from this simplified model. The numerical results of the shift can only be seen as a rough approximation when taking into account the rude simplification of the model (limitation along one dimension only, force constant to first neighbours).

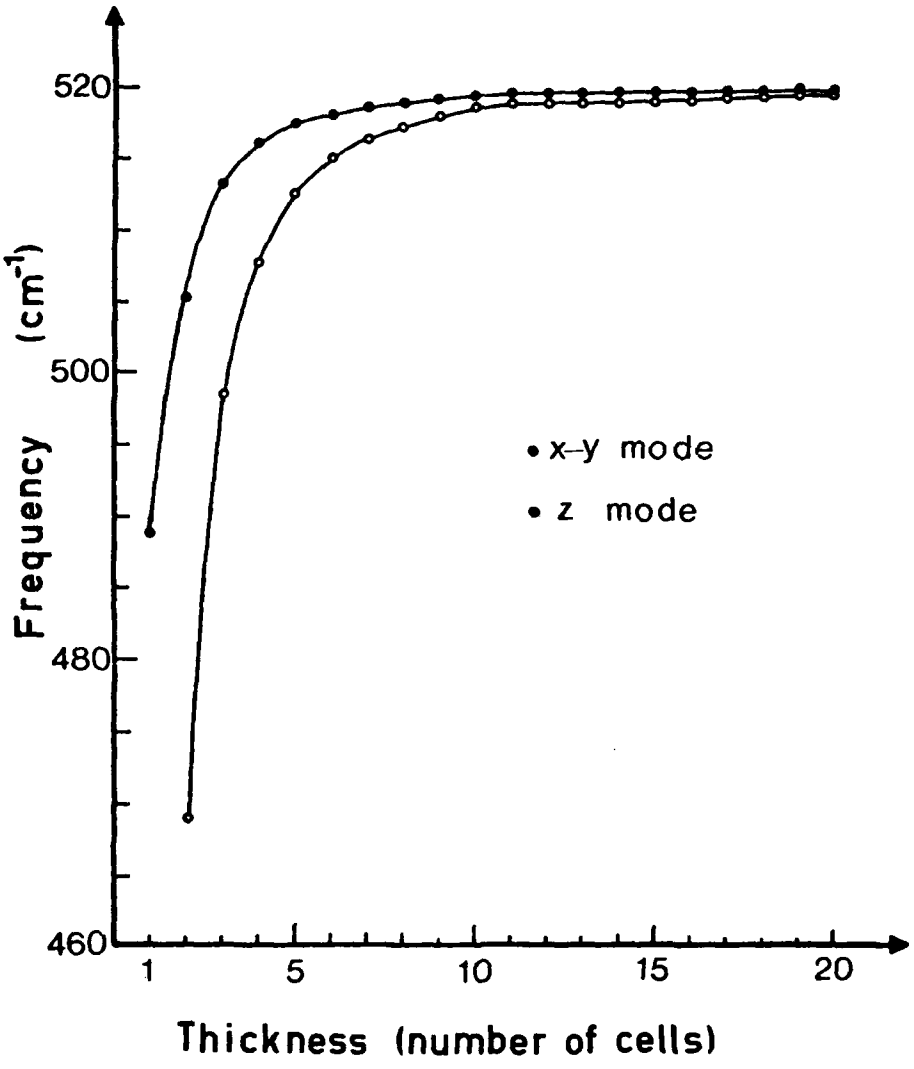


Figure 8. Theoretical variation of the frequencies of the upper modes versus the slab thickness.

To directly compare the Raman spectra observed on annealed Silicon and the results of the calculation, we have plotted on Figure 9 some kind of vibrational density obtained by adding the frequency distributions for a various number of layers with a weighting factor inversely proportional to the thickness. On the same Figure are drawn to the same scale, Raman spectra from various points of a laser annealed implanted Silicon.

For the case of very thin slab (1 to 5 cells) the frequency distribution shows a pronounced maximum near 480 $cm^{-1}$, near the maximum of the spectrum of amorphous material. Another less pronounced maximum occurs near the upper end. As the slab becomes thicker, the frequency distribution changes,the higher frequency maximum becomes sharper and the lower frequency maximum decreases and is shifted to a higher frequency.

The comparison with the Raman spectra is peculiarly impressive.

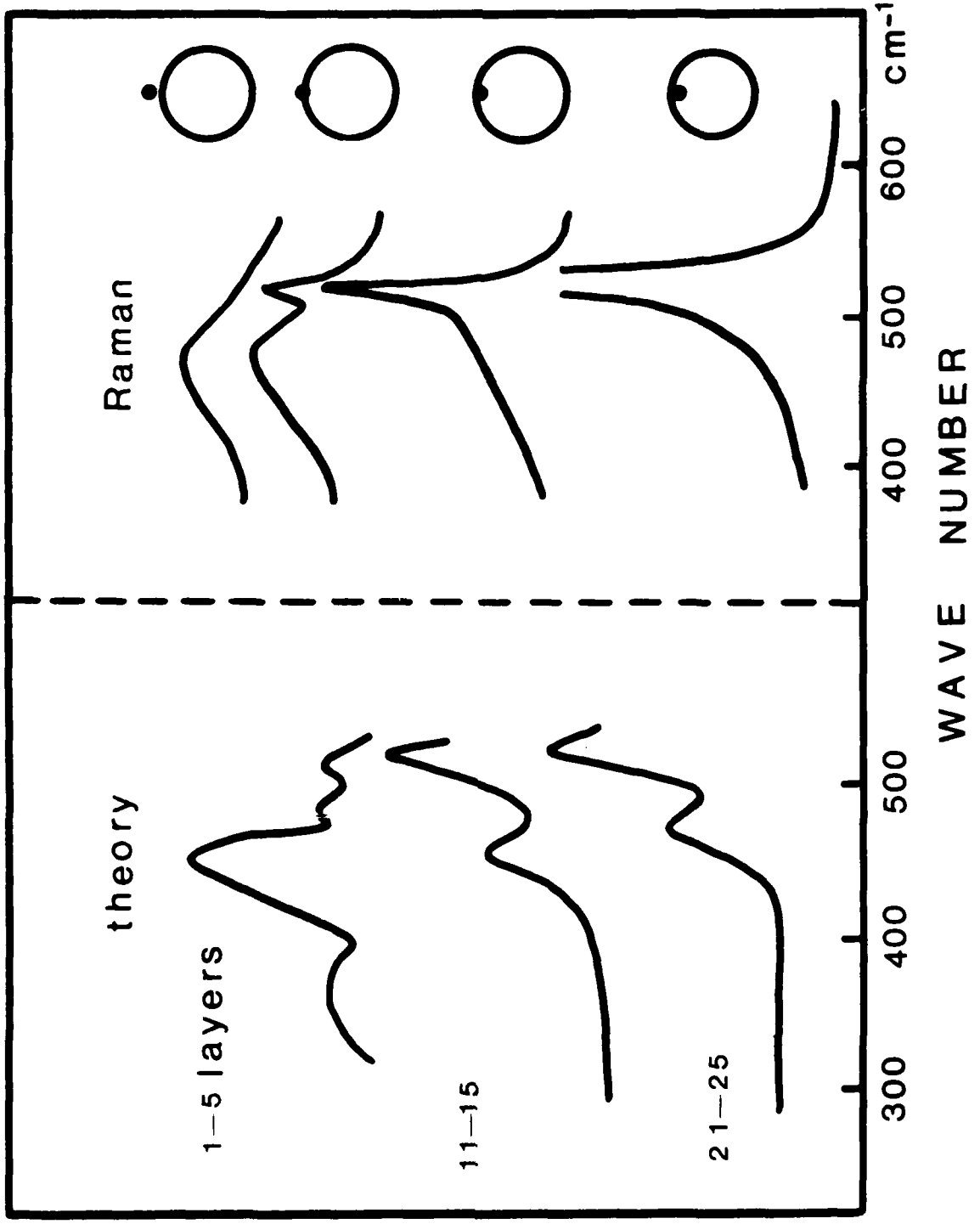


Figure 9. Theoretical weighted density of modes compared to Raman spectra of a laser annealed sample of Silicon.

## 5. CONCLUSION

Raman spectroscopy allows a fine characterisation of the disorder effect in Semiconductors. It is specifically interesting for the characterization of implantation effect, as it is one of the few non-destructive techniques. The stability of the substrate during thermal processes can be investigated as well as the annealing kninetics of the radiation damages. In this last case, Raman spectroscopy can even be used quantitatively to measure the regrowth velocity.

The extreme versatility of this technique was demonstrated once again, when the new laser annealing method was introduced. Immediately, new information was obtained concerning the topography of the annealed region. These new results have lead us to propose a lattice dynamics model of the modes of vibration of a microcrystallite. The computed data compare rather well with experimental spectra. This model, which is now limited to homopolar crystals (Silicon), will be soon extended to ionic ones (Gallium Arsenide).

## BIBLIOGRAPHY


1. - G.A. KACHORIN, E.V. NIDAEV, A.V. KHODYACHIKM, LAKOVALEVA
Sov. Phys. Semicond. 10, 1128 (1976).

2. - I.B. KHAIBULIN, E.I. SHTYRKOV, M.M. ZARIPOV, M.F. GALYA-VTDINOV, G.O. SAKIROV
Sov. Phys. Semicond. 11, 190 (1977).

3. - C.W. WHITE, J. NARAYAN, R.T. YOUNG
Science 204, 461 (1979).

4. - D.H. AUSTON, C.M. SURKO, T.N.C. VENKATESAN, R.E. SLUSHER, J.A. GOLOVCHENKO
Appl. Phys. Lett. 33, 539 (1978).

5. - J.A. VAN VECHTEN, R. TSU, F.W. SARIS, D. HOONHOUT
Phys. Lett. 74A, 417 (1979).

6. - J.A. VAN VECHTEN, R. TSU, F.W. SARIS
Phys. Lett. 74A, 422 (1979).

7. - H.W. LO, A. COMPAAN
Phys. Rev. Lett. 44, 1604 (1980).

8. - W. TSENG, J.W. MAYER, S.U. CAMPISANO, G. FOTI, E. RIMINI
Appl. Phys. Lett. 32, 824 (1978).

9. - K. KUNC
Thesis 1973, Paris.

10. - P.A. TEMPLE, C.E. HATAWAY
Phys. Rev. B7, 3685 (1973).

## ANNEXES

Publications on the subject covered by this Grant.

1. - Reprint of Solid State Communications
J.F. MORHANGE, G. KANELLIS and M. BALKANSKI
"Raman study of laser annealed Silicon".

2. - Reprint of Physical Review
G. KANELLIS, J.F. MORHANGE and M. BALKANSKI
"Effect of dimension on the vibrational frequencies of thin slab of Silicon".

3. - To be published Z. Für Physik
M. BALKANSKI, J.F. MORHANGE and G. KANELLIS
"Amorphous crystalline transition in ion implanted semiconductors".

Solid State Communications, Vol.31, pp.805-808.
Pergamon Press Ltd. 1979. Printed in Great Britain.

# RAMAN STUDY OF LASER ANNEALED SILICON*

J.F. MORHANGE, G. KANELLIS+ and M. BALKANSKI,

Laboratoire de Physique des Solides, associé au C.N.R.S.,
Université Pierre et Marie Curie
4, Place Jussieu - 75230 PARIS CEDEX 05, France

(Received 15 June 1979 by M. Balkanski)

Raman spectroscopy of laser annealed implanted Silicon shows a phonon peak shifted up to ten $cm^{-1}$ compared with a perfect crystalline sample. This shifted peak is interpreted as being due to the finite size of microcrystallites existing in the annealed region where the energy is below the fusion threshold. A simple model describing the vibrationnal properties of such crystallites has been established and compared to the experimental results.

Laser annealed amorphous Silicon layers show very different behaviour as compared to classical thermal annealed samples. It is now well established(1) that above the threshold energy which depends upon the thickness of the amorphous layer and the wavelength of the pulsed laser which is of the order of 1 $J/cm^2$, the material is fused and recrystallization occurs through a liquid phase epitaxy process allowing the recovery of a monocrystalline material. For energy below the threshold value, the annealing process is not well understood. Electronic microscopy shows evidence of polycrystalline material, the size of the microcrystallites depends upon the energy of the irradiating beam(2). Raman spectroscopy which probes the vibrationnal properties of solids gives information on the crystalline quality of the material. This technic is especially valuable at the limit between the amorphous material and the polycrystal built with crystallites of very little sizes, where Raman spectra undergoes very rapid changes. In this region ; the spectra evolves from the classical "density of states" spectrum characteristic of amorphous material to a single line spectrum characteristic of monocrystalline silicon. The frequency of this line is shifted towards lower frequencies compared to a pure monocrystalline silicon.

In order to explain the different characteristics of these spectra, we have used a simple model of a crystal, infinite along two dimensions and limited along the third one.

Single crystals wafers (100) oriented were implanted with silicon in order to avoid doping effects. Two amorphous layer thicknesses were realized 150 nm by implanting $2.10^{15}$ $Si/cm^2$ at 80 keV and 500 nm by implanting $2.10^{15}$ $Si/cm^2$ at 80 keV + $2.10^{15}$ $Si/cm^2$ under 200 keV + $2.10^{15}$ $Si/cm^2$ at 300 keV. These samples were tilted by 7° off the (100) axe to avoid channeling effects. Annealings were realized using a Q switched ruby laser, the irradiating energy was kept around $1J/cm^2$. Raman spectra were recorded using the reflection geometry. The 488 nm line of an Argon laser was foccussed onto a 80µ diameter spot. For this wavelength, the penetration depth is 1000 nm for monocrystalline silicon(3) and about 100 nm(4) for the amorphous material.

Fig. 1 presents the spectra of a 150 nm thick layer. At the center of the annealed zone where only one peak appears, situated at the true frequency of monocrystalline silicon (520.5 $cm^{-1}$). The intensity of this peak decreases while going towards the periphery. Simultaneously a shifted peak appears in the spectrum at a lower frequency, this frequency reaching 515 $cm^{-1}$ near the periphery of the annealed zone. The center of the annealed region seems then well recrystallized, the crystalline structure at the periphery being still seriously perturbed. Because of the possibility of scattering by the substrate (the amorphous thickness is 150 nm penetration depth varies between 100 and 1000 nm depending upon the state of the material), the line at the true frequency

---

+On leave from Aristotle University of Thessaloniki, Greece.

*Work performed under Grant Number DA-ERO - 78-G-002.

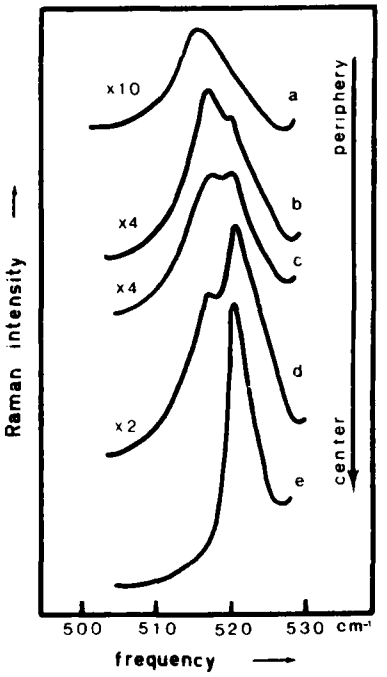


Figure 1. Raman spectra for various position of the probing laser along the diameter of a laser annealed region.
a) at the interface of the amorphous-annealed region.
b) and c) inside the annealed region.
d) near the center.
e) at the center.
The thickness of the amorphous layer was 150 nm.
Note the scale change on the vertical axe.

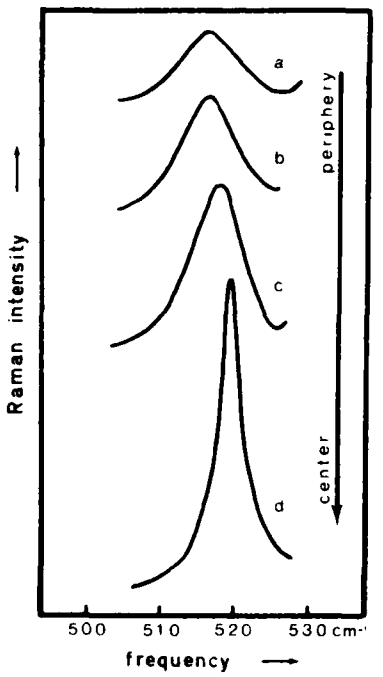


Figure 2. Raman spectra for various positions of the probing laser along the diameter of a laser annealed region.
a) at the interface of the amorphous-annealed region.
b) inside the annealed region.
c) near the center.
e) at the center.
The thickness of the amorphous layer was 500 nm.

is partially due to the monocrystalline substrate.

Fig. 2 presents spectra for a 500 nm thick layer for which the light scattering from the substrate is negligible. In this case, only one peak is evident and this peak shifts from 515 to 519 $cm^{-1}$. So, even at the center of the annealed zone, the frequency of this peak is not the true frequency of monocrystalline material. The width of this peak changes from 8 $cm^{-1}$ at the periphery to 6 $cm^{-1}$ at the center, never reaching the value for the single crystal (3.5 $cm^{-1}$) proving again the incomplete recrystallisation of the material.

Fig. 3 presents spectra of the same sample just in the neighbourhood of the limit of the annealed zone where the amorphous band is still observable. As it can be seen, this amorphous band moves towards higher frequencies until it merges with the phonon peak and remains as a tail on the lower frequency side of this peak.

Two explanations can be put forwards for these effects. Firstly, the existence of stresses in the sample could explain the frequency shift of the phonon peak. Unidirectionnal contraction of 1 % have been reported in laser annealed Boron implanted Silicon(5), but this contraction is due to the smaller size of the Boron atoms. Our samples being Silicon implanted this effect could not be large enough to account for the frequency shift observed (up to 10 $cm^{-1}$). Another kind of stresses could be of the liaxial sort, as observed just after ionic implantation(6) when lattice tends to expand. In our case, irradiation of the material will induce sudden contraction of the annealed zone, subjecting it to a negative stress which could give a frequency shift in the right direction to explain the observed shift. However, using this argument, the observed frequency variation of the amorphous band and its merging with the discrete peak cannot be explained satisfactorily.

Another explanation could be based upon the presence of microcrystal-

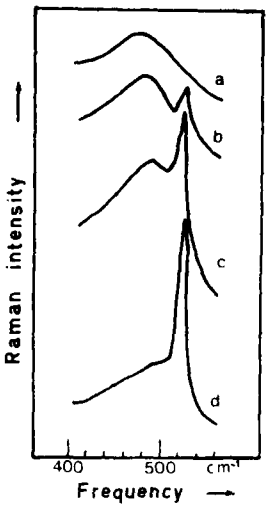


Figure 3. Raman spectra from points at each side of the edge of a laser annealed region.
a) outside the annealed region.
b) at the edge of the annealed region.
c) and d) inside the annealed region, close to the edge.

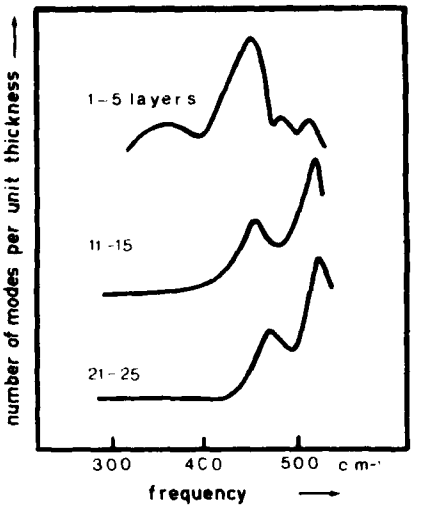


Figure 4. Weighted frequency distribution of the optical modes of a thin slab. The curves are shown as smooth lines through the calculated points.

lites of various sizes in the annealed zone. To test this hypothesis, we have compared our spectra to the frequency distribution of a finite crystal i.e. vibrations of a slab infinite along two dimensions, the number of atomic layer being only limited along the third dimension(7). Only two force constant parameter (first nearest neighbours central force and bond-bond interaction) was used and their values were fixed using the values of the frequencies of the infinite crystal. This model although very simple, gives at least a rough idea of the vibrationnal properties of a micro-crystallite.

The frequency distributions for very thin slabs have been plotted on Fig. 4. The distributions were summed on different number of atomic layers (1 to 5, 11 to 15, 21 to 25) with a weighting parameter inversely proportionnal to the thickness of the slab. The frequency distribution for the 1 to 5 layers sum shows a pronounced maximum at 480 $cm^{-1}$ near the maximum of the amorphous band of the Raman spectra. For thicker slabs, a mode at the maximal frequency is observed and the maximum of the band near 480 $cm^{-1}$ is shifted towards higher frequencies. This behaviour is then qualitatively similar to the Raman spectra observed particularly at the periphery of the annealed region (Fig. 3). Nevertheless, it must be noticed that the number of atomic layers used in this model is very small (up to 25) ; the sizes of the crystallites observed by transmission electronic microscopy was of a few hundred of Angströms(2) which is much larger than the few atomic layers used in the model. A complete computation on a crystal limited along the three dimensions could perhaps give more realistic results.

## REFERENCES

1. D.H. AUSTON, C.M. SURKO, T.N.C. VENKATESAN, R.E. SLUSHER and J.A. GOLOUCHENKO Appl. Phys. Lett. 33, 437 (1978).

2. W.F. TSENG and J.F. MAYER, S.U. CAMPISANO, G. FOTI and E. RIMINI, Appl. Phys. Lett. 32, 825 (1978).

3. W.C. DASH, R. NEWMAN, Phys. Rev. 99, 1151 (1955).

4. M.H. BRODSKY, R.S. TITLE, K. WEISER and G.G. PETIT, Phys. Rev. B1, 2632 (1970).

5. B.C. LARSON, C.W. WHITE and B.R. APPLETON, Appl. Phys. Lett. 32, 801 (1978).

6. K. SESHAN and E.P. EERNISSE, Appl. Phys. Lett. 33, 21 (1978).

7. G. KANELLIS, (to be published).

PHYSICAL REVIEW B VOLUME 21, NUMBER 4 15 FEBRUARY 1980

# Effect of dimensions on the vibrational frequencies of thin slabs of silicon

G. Kanellis,* J. F. Morhange, and M. Balkanski
*Laboratoire de Physique des Solides de l'Université Pierre et Marie Curie associé au CNRS, 4 place Jussieu, 75230 Paris Cedex 05, France*
(Received 23 July 1979)

Calculated frequencies of the long-wavelength vibrations of thin slabs of silicon parallel to the (111) plane show that the in-plane modes decrease almost exponentially in frequency with decreasing thickness of the slab. The out-of-plane modes have frequencies lower than the in-plane modes and decrease in the same fashion as the slab becomes thinner. This result is consistent with the observation that the Raman-active mode shifts toward lower frequencies in laser-annealed, ion-implanted silicon when the recrystallization is not perfect.

## I. INTRODUCTION

In recent years growing interest has developed in materials that are not infinite crystals. Polycrystalline semiconductor heterostructures and materials have given rise to a great deal of fundamental work related to some of their exceptional properties. Amorphous and polycrystalline states are successive steps in the recrystallization process of ion-implanted materials when specific doping is intended for some particular use.

To account for the observation[1] that in laser-annealed ion-implanted silicon, depending on the degree of recrystallization, the Raman-active mode shifts from 520 $cm^{-1}$, the frequency of the $\Gamma$-point optical mode in a perfect crystal, to 516 $cm^{-1}$, we attempt to attribute this shift to the effect of dimensions on the vibrational properties in small crystallites of imperfectly recrystallized silicon.

It is now well established that real crystals, when their dimensions are relatively small, show, in addition to the normal modes of the infinite lattice, surface modes and effects of dimension: when the dimensions become extremely small only the surface modes persist.

In ionic crystals of finite thickness,[2] one finds two classes of modes: Those of the oscillatory spatial dependence and frequencies equal to the normal transverse- (TO) and longitudinal-optical (LO) frequencies at $\vec{q}=0$, in an infinite crystal, and those with an exponential dependence on distance across the slab and frequencies between $\omega_{LO}$ and $\omega_{TO}$. More recent calculations[3] of the long-wave optical vibrational modes in finite ionic crystals of arbitrary shape have led to the same conclusions: In finite specimens there exist transverse and longitudinal bulk modes as well as surface modes which are neither transverse nor longitudinal and which have intermediate frequencies.

When the expansion of the displacement in plane waves is not used in the calculation of the vibrational frequencies of finite one-dimensional lattices,[4] one shows that the free ends produce "surface" modes of vibrations with frequencies in the forbidden gap between the optical and acoustical branches.

Surface modes and size effects have been calculated for many different systems. In a semi-infinite lattice[5] with the harmonic approximation, the normal modes are classified into "bulk" and "surface" modes. The surface modes exhibit an exponential decay of their amplitude away from the free surface because they have a complex wave-vector component normal to the surface. The frequencies of these modes lie in intervals which have, at most, their end points in common with intervals where bulk modes occur at the same transverse wave vectors.

Calculations for the surface mode in diamond and zinc-blende lattices[6] have shown that the details of the modes depend strongly on the structure of the surface: A very detailed knowledge of the geometric surface structure is necessary to make definite statements on frequencies of surface modes.

Our purpose here is to account for the variation of normal-mode frequencies with dimensions in a polycrystalline structure. A detailed calculation is impossible at present because of the poor knowledge of the exact structure of the interfaces. Therefore we believe that at this stage a useful exercise would be to give the general features of the observed correlation between the frequency shift of the Raman-active mode and crystallite dimensions on the basis of a very simple model.

## II. THEORETICAL MODEL

For the purpose of examining the effect of the finite size of a homopolar crystal on the frequencies of the vibrational modes, we consider the simplest case, e.g., the case of a thin slab

 

extended to infinity in two directions. The slab is considered to consist of a number of layers, each of which has the thickness of a unit cell. In such a structure, the periodicity of the lattice is conserved along the two directions, and, consequently, the atomic displacements parallel to these directions can be expanded in plane waves, and the periodic boundary condition can be applied. Along the third direction neither of the above considerations is possible, and the sequence of cells along that direction is treated merely as one unit cell. As a result, the number of independent interactions increases considerably, for we have to account for interactions between plane lattices rather than three-dimensional ones. In fact, for a slab consisting of $N$ unit-cell layers with $n$ atoms per unit cell, the dynamical matrix needed to provide the vibrational frequencies is of $3nN \times 3nN$ dimensions. Associated with the above structure is a two-dimensional reciprocal lattice which displays a symmetry depending upon the orientation of the slab in the three-dimensional lattice. The corresponding two-dimensional Brillouin zone is a section of the three-dimensional one. Some reduction of the above-mentioned dynamical matrix for special points of the Brillouin zone may be possible if the orientation of the slab is chosen to be across directions of the crystal of high symmetry.

For the fcc lattice in which the group IV elements (Fig. 1) crystallize, the (111) plane is favorable, for it displays a relatively high symmetry and, moreover, the plane lattices parallel to that plane are described by two of the three unit vectors of the three-dimensional lattice. A new coordinate system $Ox'y'z'$ chosen so that the $Ox', Oy'$ axes are coplanar with the slab while the $Oz'$ direction is perpendicular to it, e.g.,

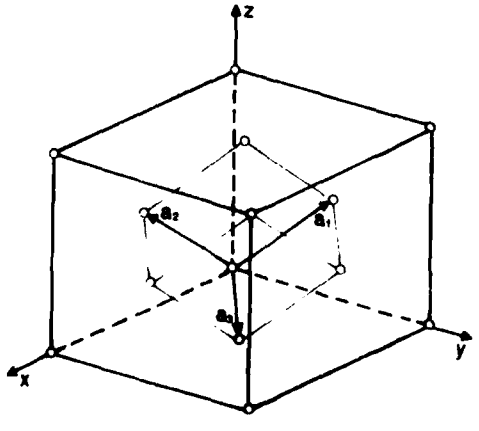


FIG. 1. Schematic representation of the face-centered-cubic lattice.

$$\vec{x}_0' = \frac{\vec{a}_1 - \vec{a}_2}{|\vec{a}_1 - \vec{a}_2|}, \quad \vec{y}_0' = \frac{\vec{a}_1 + \vec{a}_2}{|\vec{a}_1 + \vec{a}_2|}, \quad \vec{z}_0' = \frac{\vec{a}_1 \times \vec{a}_2}{|\vec{a}_1 \times \vec{a}_2|}, \tag{1}$$

where $\vec{a}_1, \vec{a}_2$ are the primitive lattice vectors.

The new coordinates of the atoms are given by the relations

$$\begin{pmatrix} x' \\ y' \\ z' \end{pmatrix} = H \begin{pmatrix} x \\ y \\ z \end{pmatrix}, \tag{2}$$

where $H$ is the transformation matrix

$$H = 6^{-1/2} \begin{pmatrix} -3^{1/2} & 3^{1/2} & 0 \\ 1 & 1 & 2 \\ 2^{1/2} & 2^{1/2} & -2^{1/2} \end{pmatrix}. \tag{3}$$

If the space group $G$ of the original (three-dimensional) structure is symmorphic a similar transformation of the form

$$R_i' = H R_i H^{-1} \tag{4}$$

provides the new representations $R_i'$ of the group elements. If the initial space group is nonsymmorphic, the associated translation vector $\vec{v}$ has to be transformed accordingly:

$$\vec{v}' = H\vec{v}.$$

Among the rotations in the new representation $R_i'$ we choose only those which are associated with a translation $\vec{v}'$ whose $z$ component is zero (if any), and which have the form

$$R_i' = \begin{pmatrix} & & 0 \\ & S_i & 0 \\ 0 & 0 & 1 \end{pmatrix}, \tag{5}$$

where $S_i$ is a $2 \times 2$ matrix.

The group $G'$ of the so chosen elements is the "space" group of the new two-dimensional structure (slab) and can be used to provide the form of the force-constant matrices and the relations between the elements of the dynamical matrix.[7]

The elements of the dynamical matrix are defined by

$$D_{\alpha\beta}\begin{pmatrix} l_3 & l_3' \\ k & k' \end{pmatrix}\Big|\vec{q}\Big) = \exp\left\{-i\vec{q}\left[\vec{x}\begin{pmatrix} l_3 \\ k \end{pmatrix} - \vec{x}\begin{pmatrix} l_3' \\ k' \end{pmatrix}\right]\right\}(m_k m_{k'})^{-1/2} \times \sum_{ll'} \Phi_{\alpha\beta}\begin{pmatrix} l & l' \\ k & k' \end{pmatrix} \times \exp\left\{-i\vec{q}\left[\vec{x}\begin{pmatrix} l_1 \\ l_2 \end{pmatrix} - \vec{x}\begin{pmatrix} l_1' \\ l_2' \end{pmatrix}\right]\right\}, \tag{6}$$

where the wave vector $\vec{q}$ refers to the two-dimensional Brillouin zone, and

$$\vec{x}\begin{pmatrix} l_1 \\ l_2 \end{pmatrix} = l_1\vec{a}_1 + l_2\vec{a}_2 \tag{7a}$$

describes the points of the two-dimensional infinite lattice and

$$\vec{x}\begin{pmatrix} l_3 \\ k \end{pmatrix} = l_3\vec{a}_3 + \vec{x}(k) \tag{7b}$$

describes the positions of the atoms within a "unit" cell, consisting of the sequence of unit cells of the original structure along the direction $\vec{a}_3$.

In what follows we are merely interested in the long-wavelength vibrations, e.g., $\vec{q} \sim 0$, so the exponential factors drop out.

The position vectors of the atoms and the dynamical matrix can be expressed in either of the above-mentioned coordinate systems $Oxyz$ (unprimed symbols) or $Ox'y'z'$ (primed symbols) by the same relations (6 and 7), provided the lattice primitive vectors $\vec{a}_i$ are expressed accordingly. In the system $Oxyz$ these vectors are given by the relation

$$\begin{pmatrix} \vec{a}_1 \\ \vec{a}_2 \\ \vec{a}_3 \end{pmatrix} = \frac{a}{2}\begin{bmatrix} 0 & 1 & 1 \\ 1 & 0 & 1 \\ 1 & 1 & 0 \end{bmatrix}\begin{pmatrix} \vec{x}_0 \\ \vec{y}_0 \\ \vec{z}_0 \end{pmatrix}, \tag{8}$$

where $a$ is the lattice constant.

The two representations of the dynamical matrix for $\vec{q} = 0$ are related by the similarity transformation

$$D'(0) = TD(0)T^{-1}, \tag{9}$$

where $T$ is an orthogonal matrix of the same order as $D$ and whose elements are

$$T_{\alpha\beta}\begin{pmatrix} l_3 & l_3' \\ k & k' \end{pmatrix} = H_{\alpha\beta}\delta_{l_3 l_3'}\delta_{kk'}. \tag{10}$$

Using the corresponding point group $G_0'$ of the above-defined space group $G'$, we find that the interactions between the plane lattices are expressed for $\vec{q} = 0$ by a matrix

$$D\begin{pmatrix} l_3 & l_3' \\ k & k' \end{pmatrix}$$

of the form

$$D\begin{pmatrix} l_3 & l_3' \\ k & k' \end{pmatrix} = \begin{bmatrix} A & B & -B \\ B & A & -B \\ -B & -B & A \end{bmatrix}. \tag{11}$$

Using the transformation (9) we obtain the diagonal form

$$D'\begin{pmatrix} l_3 & l_3' \\ k & k' \end{pmatrix} = \begin{bmatrix} A-B & 0 & 0 \\ 0 & A-B & 0 \\ 0 & 0 & A+2B \end{bmatrix}. \tag{12}$$

This form implies that the solutions for any slab having the above orientation are separated into two groups, one doubly degenerate containing the solutions corresponding to modes which vibrate in the two directions where the slab extends to infinity ($xy$ modes), and one nondegenerate containing the solutions corresponding to vibrations perpendicular to the surfaces of the slab. This reduction by a factor of 3 of the dynamical matrix due to the orientation of the slab simplifies the computations.

For the purpose of comparing the frequencies of the above two types of solutions for a slab with the frequencies of an infinite lattice in the case of silicon, we calculated these frequencies on the basis of the following valence-force-field model. We assume only first-neighbor central interactions (force constant $\lambda$) and bond-bond interactions of the type proposed by Clark, Gazis, and Wallis[8] (force constant $\gamma$).

It is well known that such a model is inadequate to reproduce with accuracy the experimentally found dispersion curves for Si, because even a valence-force-field model with six parameters describing forces extended to the third neighbor gives higher frequencies for the acoustical branches.[9] As has been shown by Weber,[10] Coulomb interactions through charges localized on the bonds have to be introduced to describe properly the lowering and the flatness of these branches.

Nevertheless, we think that the proposed model is sufficient for the purpose of studying to a first approximation the effect of the finite size of the slab on the frequencies of vibrations. According to that model, the potential energy of the lattice is written as

$$\Phi = \frac{1}{2}\sum_{ij}\lambda(dr_{ij})^2 + \frac{1}{3!}\sum_{ijj'}\gamma r_0^2(d\theta_{ijj'})^2, \tag{13}$$

where the first sum extends over all first-nearest neighbors and the second sum over all angles of bonds for each atom.

Because the forces considered are extended only to second-nearest neighbors, it is evident that the interaction matrices

$$\Phi\begin{pmatrix} l_3 & l_3' \\ k & k' \end{pmatrix}$$

between the same pair of atoms $k,k'$ are identical with those for the infinite structure, if at least one of the atoms lies at a distance from the surfaces of the slab greater than the thickness of the primitive unit cell measured perpendicular to the surface; i.e., only the forces exerted on the atoms on the first two lattice planes from the surfaces are perturbed if no change of equilibrium positions of the atoms due to the presence of the surface is assumed.

Finally, we note that the Brillouin zone corresponding to the slab structure is a section of the three-dimensional one for the fcc lattice through the center perpendicular to the vector $\vec{b}_3$.

## III. RESULTS AND DISCUSSION

The values of the two parameters involved have been obtained by a fitting to the frequencies of the TO modes at the points $\Gamma$, $X$, and $L$ of the infinite structure. The experimental values of these frequencies, the calculated ones, and the values of the parameters are given in Table I. The reason for using only the frequencies of the optical modes is that the frequencies of the acoustical modes at the points $X$ and $L$ are lower than predicted by such a model as discussed in the preceeding paragraph.

Using these values we have calculated the frequencies of the vibrational modes for slabs having thickness from 1 to 50 unit cells. The results obtained can be described as follows.

The $xy$ modes, e.g., modes of $\vec{q}=0$ vibrating parallel to the surface of the slab, are grouped in two regions separated by a large gap which is almost equal to the gap between the TA and TO phonons of the point $L$ of the three-dimensional structure. This means that all these modes should belong to the two branches of transverse phonons across the $\Lambda$ direction. This is particularly true in the limit of a large number of cells across the $z$ direction. For a slab having the thickness of only one cell, the gap is reduced by approximately 2 $cm^{-1}$ from the three-dimensional one.

TABLE I. Transverse-optical frequencies for the points $\Gamma$, $L$, and $X$ in the Brillouin zone (BZ).

| Point in the BZ | TO frequencies($cm^{-1}$)[a] Experiment | Calculated |
|---|---|---|
| $\Gamma$ | 520 | 520 |
| $L$ | 491 | 491.5 |
| $X$ | 462 | 461.3 |

[a] Values of parameters used in the calculations: $\lambda = 1.296$ mdyn/Å, $\gamma = 0.047$ mdyn/Å.

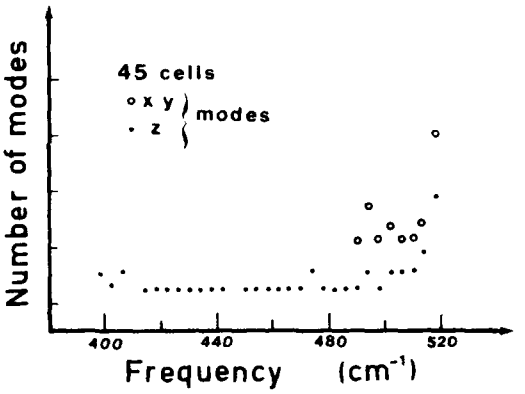


FIG. 2. Distribution of the optical in-plane modes: $xy$ modes represented by O, and of out-of-plane modes: $z$ modes represented by ● as a function of frequency.

All the modes of the upper group are of optical type, e.g., every pair of atoms in each cell moves in antiphase, while all the modes of the lower group are of acoustical type. The distribution of the "optical" modes shows two peaks near the limits of the frequency interval in which they are contained (Fig. 2). The distribution of the acoustical modes is rather constant, except near the

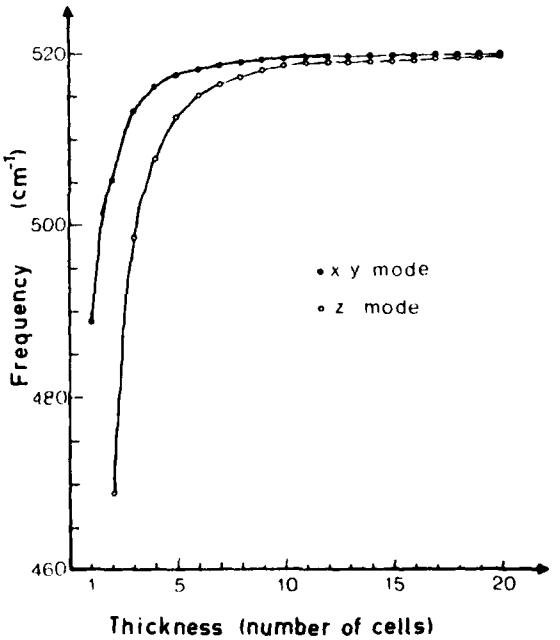


FIG. 3. Frequency variation of the higher-frequency optical mode for the $xy$ modes as a function of the number of cells, i.e., thickness of the slab, rising exponentially toward the limit frequency of the $\Gamma$-point TO mode of the three-dimensional lattice. The higher-frequency $z$ mode shows the same variation although lower in frequency.

upper end of the interval where it shows a peak.

The higher frequency of the optical modes corresponds to the one of the Γ point. For a slab having the thickness of only one cell, this frequency lies near the peak of the amorphous material spectrum and varies almost exponentially with the thickness towards the Γ frequency of the infinite lattice (Fig. 3).

The $z$ modes, e.g., the modes whose displacements are along the $z$ axis, have frequencies which are distributed between zero and the Γ-mode frequency, in two groups with a gap between them almost equal to the gap between the LO and LA frequencies of the point $L$ of the three-dimensional lattice.

Again the vibrations of the higher-frequency group are of optical type and belong to the LO branch of the perfect crystal, while the vibrations of the lower-frequency group are of acoustical type, except the one with the higher frequency in this group which is again of optical type.

The distribution of the $z$ modes of both types at the corresponding intervals is similar and is almost constant over the frequency range, showing only a peak at the upper end of the range.

The higher-frequency optical mode corresponds again to the Γ-point optical mode of the perfect crystal. The dependence of its frequency on the thickness of the slab is similar to that of the corresponding $xy$ mode with the difference that the values are lower (Fig. 3).

Weighted frequency distributions of $xy$ and $z$ optical modes with a weighting factor inversely proportional to the thickness of the slab are shown in Fig. 4. For the case of very thin slabs 1 to 5 unit cells thick [Fig. 4(a)], the frequency distribution shows a pronounced maximum between 480–490 $cm^{-1}$ near the maximum of the spectrum of amorphous material. Another less pronounced maximum occurs near the upper end. For the case of thicker slabs (11–15 unit cells thick) the frequency distribution of optical modes changes, showing the higher-frequency maximum more pronounced than the lower-frequency one [Fig. 4(b)]. Finally, the frequency distribution of even thicker slabs (21–25 unit cells thick) exhibits analogous features except that the higher-frequency maximum becomes more pronounced,

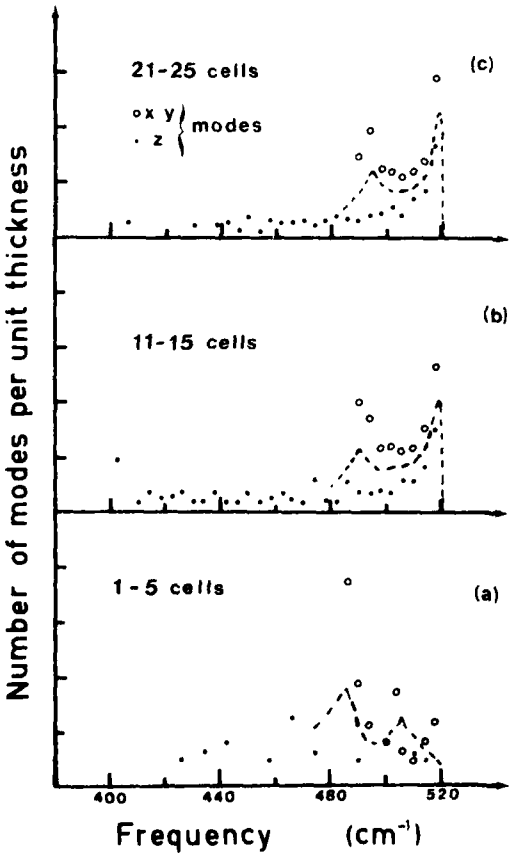


FIG. 4. Weighted frequency distributions of $xy$ represented by O and $z$ optical modes represented by ● with a weighting factor inversely proportional to the thickness of the slab. Number of modes per unit cell as a function of frequency. (a). For very thin slabs: 1 to 5 cells thick. (b). For slabs having a thickness of 11 to 15 cells. (c). For slabs 21 to 25 cells thick.

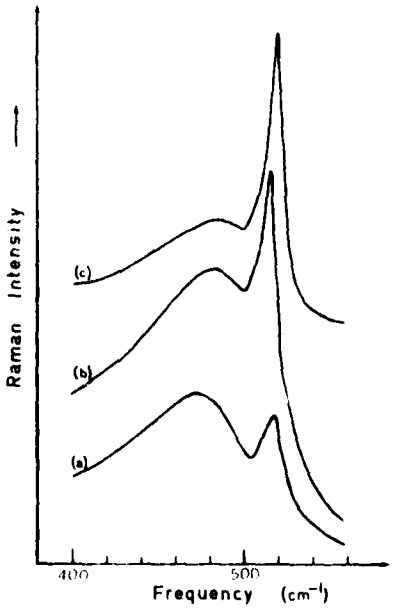


FIG. 5. Raman spectra of laser-annealed ion-implanted Si from three regions with partial recrystallization: (a), (b), and (c) partially recrystallized with grains of increasing size.

and the one at lower frequency is shifted to higher frequencies.

These features are exactly what has been observed in the Raman spectra of laser-annealed ion-implanted Si, in the intermediate recrystallization stage. These spectra can be explained if a distribution of very small crystallites of different sizes is assumed. As the distribution of crystallites moves towards larger sizes, the observed spectrum shifts from the one of the amorphous material to that exhibiting a second peak near the upper end, superimposed on the amorphous material spectrum and finally, to a spectrum showing only one peak of practically the same frequency as that of the perfect crystal, followed by a tail towards lower frequencies. This experimental results are summarized in Fig. 5.

## IV. CONCLUSIONS

We have calculated the frequencies of the long-wavelength vibrations of thin slabs of silicon, parallel to the (111) plane, on the basis of a very simple valence-force-field model with two parameters for the purpose of studying the effect of the finite thickness of the slab on the vibrational frequencies of small homopolar crystals. We found that all of the modes belong to the certain branches of phonons of the perfect crystal, but have frequencies generally lower, depending on the thickness of the slab. Weighted frequency distributions of the optical-mode frequencies for slabs with different thicknesses display the main features of the Raman spectra of laser-annealed ion-implanted silicon when the recrystallization is imperfect.

## ACKNOWLEDGMENT

This research was supported in part by the European Research Office of the U. S. Army Grant No. DA ERO-78-G-002.

*Permanent address: First Laboratory of Physics, Aristotle University of Thessaloniki, Greece.

[1]F. Morhange, G. Kanellis, M. Balkanski, J. F. Peray, J. Icole, and M. Croset, in *Laser-Solid Interactions and Laser Processing*–1978 (*Materials Research Society, Boston*), edited by S. D. Ferris, H. J. Leamy, and J. M. Poate (AIP, New York, 1978), p. 429.

[2]R. Fouchs and K. L. Kliewer, Phys. Rev. 140A, 2076 (1965).

[3]R. Engelman and R. Ruppin, J. Phys. C 1, 614 (1968).

[4]R. F. Wallis, Phys. Rev. 105, 540 (1957).

[5]T. E. Feuchtwang, Phys. Rev. 155, 731 (1967).

[6]W. E. W. Ludwig, J. Appl. Phys. Suppl. 2, Pt. 2, 879 (1974).

[7]J. L. Warren, Rev. Mod. Phys. 40, 38 (1968).

[8]B. C. Clark, D. C. Gazis, and R. F. Wallis, Phys. Rev. 134, A1486 (1964).

[9]R. Tubino, L. Piseri, and G. Zerbi, J. Chem. Phys. 56, 1022 (1972).

[10]W. Weber, Phys. Rev. B 15, 4789 (1977).

# AMORPHOUS CRYSTALLINE TRANSITION IN ION IMPLANTED SEMICONDUCTORS

M. BALKANSKI,,J.F. MORHANGE and G. KANELLIS

1980

# AMORPHOUS CRYSTALLINE TRANSITION IN ION IMPLANTED SEMICONDUCTORS

M. BALKANSKI, J.F. MORHANGE and G. KANELLIS

Laboratoire de Physique des Solides, associé au C.N.R.S.,
Université Pierre et Marie Curie
4, Place Jussieu, 75230 PARIS CEDEX 05

ABSTRACT

Recrystallization of amorphous semiconductors obtained by ion implantation is investigated by light scattering spectroscopy. Thermal annealing as well as laser annealing is shown to proceed trough the formation of small crystallites. Lattice dynamics calculations compared to the distribution of crystallites in the laser annealed area show the effect of dimensions in the amorphous crystalline transition. Short pulse laser annealing is considered as first creating an electron hole plasma which condensates into droplets and initiates nucleation by energy transfert to the lattice.

## 1. - INTRODUCTION

Ion implantation has openned in recent years the hope of a new technology in semiconductor devices. Evident advantages in precision and efficiency are compensated by the fact that by ion implantation the semiconductor becomes amorphous and needs to be recrystallized in order to recover the perfect crystal properties necessary for the performances of modern devices. We are presenting here a certain number of results on the recrystallization processes and a few prospective remarks.

Two different technics are used for the recrystallization of the amorphous implanted layer : thermal and laser annealing. Many previous investigations by different methodes have lead to propose mechanisms for recrystallization often inspired by the idea of epitaxial grow. Using laser Raman spectroscopy for the characterization of the amorphous and the crystalline state by which we determine the local crystallographic order, we are inclined to suggest that in neither of the technics used to recrystallize amorphous implanted semiconductors, melting of the lattice could be involved.

Analysis of the experimental results presented here suggest that in thermal annealing an activation energy for recrystallization is determined which might well be an activation energy needed for the displacement of atoms in the amorphous material into favourable positions to initiate nucleation and crystal grow.

When laser annealing is investigated one observes a characteristic topology for the distribution and size of the crystallites with regard to the shape of the laser irradiated area. Outside of the limit of the power laser spot the material remains amorphous and the Raman spectrum observed is that characteristic of the amorphous state.

At the edge of the annealed area a polycrystalline stucture is observed with size and density distribution of crystallites systematically changing when moving toward the center of the annealed area. At the center one has a perfect crystalline region and the

crystallite size decreases when going toward the periphery. We have developped a simple model to account for the effect of dimensions and to compare theoretically calculated frequency distributions of vibrational modes with the size distribution of microcrystallites.

Our observations on the occurence and the distribution of vibrational modes of particular frequencies and the polycrystalline topography which can be infered from these results leads to think that short pulse laser annealing proceeds through the initial creation of a dense electron hole plasma by the radiation field which condenses into electron hole droplets and favors through energy exchange with the lattice the atomic displacements into sites favourable for nucleation and grow into small crystallites. The size of crystallites and their distribution depends on the energy density distribution of the laser pulses.

## 2. - THERMAL ANNEALING

### 2.1. Thermal annealing of implanted silicon

#### 2.1.1. Characterisation of single crystal and amorphous silicon by light scattering

Silicon crystalizes in diamond structure with two atoms per unit cell. Only one optical mode triply degenerate is Raman active giving in a light scattering spectrum a peak at $\omega$ = 520,5 $cm^{-1}$ having a width of $\Delta\omega$ = 3,5 $cm^{-1}$.

Ion implantation at relatively hight doses produces two types of effects : light ions such as B, C, N, introduces a high degree of disorder but the material after implantation remains still crystalline ; heavy ions completely destroy the crystal lattice and the material becomes amorphous. The light scattering spectrum of amorphous silicon is drastically different of that of the single crystal : the sharp peak at 520,5 $cm^{-1}$ completely disappears and instead one observes a broad band spread over a wide spectral range with two singularities, one centered at 480 $cm^{-1}$ and another one of lower intensity centered at 150 $cm^{-1}$. These two features correspond to maxima in the optical and acoustical density of modes respectively. As an example[1], Figure 1 shows the Raman spectrum of silicon implanted with arsenic.

The thickness of the implanted layer which has been rendered amorphous can be determined in a light scattering experiment by taking into consideration the absorption coefficient $\alpha_a$ of the amorphous material and by considering that the interface between amorphous and crystalline areas is well defined and abrupt.

If the light beam is scattered at normal modes of the crystalline substrate and then crosses an amorphous layer of thickness d having an absorption coefficient $\alpha_a$, its incident intensity $I_o$ will be altered by a factor $\exp(-2\alpha_a d)$ and will be given by

$$I = I_o (1-R_a)^2 (1 - R_{ax})^2 S_x \exp(- 2 \alpha_a d) \qquad (2.1)$$

The scattering intensity in a layer of perfect crystal in this frequency region will be :

$$I_x = I_o (1 - R_x)^2 S_x \qquad (2.2)$$

here $R_x$, $R_a$ and $R_{ax}$ are the reflectivity coefficients at the crystal-air amorphous-air and amorphous-crystal interfaces, and

$S_x$ is the scattering cross sections of the crystalline material.

The ratio of the two scattered beams is then given by :

$$\text{Log } \frac{I}{I_x} = \text{Log } \frac{(1 - R_a)^2 (1 - R_{ax})^2}{(1 - R_x)^2} - 2 \alpha_a d \qquad (2.3)$$

The first term in the second member is independent of the wavelength of the light in the region of interest and the curve Log $I/I_x = f(\alpha_a)$ is a straight line with slop 2d.

The thickness[1] of the amorphous layer in silicon implanted with $10^{14}$ ions of $P/cm^2$ under 70 KeV as determined by this method is 1000 Å and with $10^{16}$ ions of $As/cm^2$ is 500 Å.

### 2.1.2. Isochronal annealing of implanted silicon

Above a given implantation dose, which depends on the mass of the implanted ions, and to which we shall refer as the amorphization threshold, the Raman spectrum of the implanted silicon is entirely that of the amorphous material and shows no trace from the peak at 520,5 $cm^{-1}$. This is the case of the top curve in Figure 2 before termal annealing. When termal annealing is performed during one hour at 525° C the peak at 520,5 $cm^{-1}$ characteristic of the crystal appears. When the annealing temperature grows up, the intensity of the crystalline peak increases. The ratio of the integrated intensity of the peak at 520,5 $cm^{-1}$ to that of pure non implanted material determine the degree of recrystallization by termal annealing. The phase transi-

tion between amorphous and crystalline silicon is a slow process at temperatures far from the melting point.

### 2.1.3. Isothermal annealing of implanted silicon

When the annealing temperature is kept constant and the duration of annealing is progressive the Raman peak giving the proportion of material which recrystallizes is steadily increasing with time as shown in Figure 3.

## 2.2. Thermal annealing in GaAs

### 2.2.1. Characterization of crystalline and amorphous GaAs

As in the case of silicon the light scattering of amorphous GaAs taken just after ion implantation shows a broad band spectrum. The Raman spectrum of blende structure GaAs single crystals at the contrary consists of two peaks corresponding to the transverse optical (TO) and the longitudinal optical (LO) normal modes of vibrations at the center of the Brillouin zone.

In a back scattering experiment both modes are not equally allowed for all crystallographic faces. For a reflection at a face (100) TO is forbiden and LO is allowed whereas for the face (110) TO is allowed and LO is forbiden and for the face (111) both are allowed.

In Figure 4 are shown the light scattering spectra of crystalline and amorphous GaAs. It is obvious that a clear distingtion can be made between the crystalline and the amorphous states by means of Raman spectroscopy. The amorphous material investigated here is obtained by implanting arsenic in GaAs at a dose of $10^{16}$ ions/cm$^2$ at 60 KeV.

### 2.2.2. Isochronal annealing

When termal annealing is performed the progressive recrystallization of the amorphous material can be followed by Raman spectroscopy. Figure 5 are shown the Raman spectra of GaAs,

implanted with phosphorous at a dose of $10^{16}$ atoms/$cm^2$ under 60 KeV, after annealing at various temperatures during 30 minutes. The annealing is characterized by the appearance of the TO and LO phonon peaks whose intensity grows with temperature. Above 600° C no further evolution of the spectra is observed which indicates that recrystallization is achieved after 30 minutes at 600° C. In the temperature range between 450 and 600° C two additional peaks show up at frequencies 200 and 257 $cm^{-1}$. These two frequencies correspond to the modes $A_{1g}$ and $E_{1g}$ of arsenic crystallized in the trigonal structure[2]. The appearence of these two peaks indicates arsenic exodiffusion at the GaAs surface for temperature above 450° C and subsequent evaporation of the arsenic from the surface which is considerably dommaged at temperatures approaching 600° C when the samples are not protected during termal treatment.

### 2.2.3. Isothermal annealing

The recrystallization kinetics can be more efficiently studied in an isothermal annealing. Under the assumption that the recrystallization process can be regarded as a solid phase epitaxy like in silicon and germanium[3] the speed of recrystallization can be determined. In order to be able to do this determination one has to suppose that after implantation the interface between single crystal substrate and amorphous implanted region is abrupt. The speed of recrystallization will then be defined as the distance covered by this interface per unit time during the annealing. The method used in this determination is shown schematically in Figure 6. In this Figure the horizontal solid line represents the plane for which the reflectivity $R_a$ of the amorphous GaAs is measured and the dotted horizontal line represents the plane for which the reflectivity $R_{ax}$ at the interface amorphous-crystal is determined.

If now we designate by $S_x$ the light scattering cross section of the crystalline GaAs and by d the thickness of the amorphous layer the measured Raman intensity of a completely crystalline sample will be the equation (2.2).

For a sample of thickness d the Raman intensity scattered by the crystalline substrate at the interface crystal-amorphous will be the equation (2.1).

The ratio of these two expressions eliminates $S_x$. $R_a$ and $R_x$ can be measured. $R_{ax}$ can not be measured and is not knowed but it can be agreed that this is a very small quantity compared to $R_x$ and $R_a$ and therefore be neglected without affecting the results.

The absorption coefficient of the amorphous layer is determined by the following method.Considering the ratio

$$r = \frac{(1 - R_a)^2}{(1 - R_x)^2} \exp(-2\alpha_a d)$$

the quantity to be determined is the thickness of the amorphous layer d. For this purpose a sample of GaAs is implanted with arsenic at a dose of $10^{16}$ atoms/cm$^2$ under 60 KeV and the tickness determined as $d = R_p + \Delta R_p$ where $R_p$ is the projection range and $\Delta R_p$ the straggling range . A fairly good value in this case seems to be d = 380 Å. With a laser beam of $\lambda$ = 5145 Å, $\alpha.d = 2.06$ and the calculated absorption coefficient $\alpha_a = 5.4.10^5$ cm$^{-1}$ is one order of magnitude higher then the absorption coefficient of crystalline GaAs at the same wavelength ($\alpha_x = 8.10^4$ cm$^{-1}$).

With this absorption coefficient it is now possible to calculate the recrystallization speed. Recrystallization speed for As implanted GaAs is determined at temperatures of 200° C, 220° C and 240° C. On Figure 7 is presented a plot of Log $\frac{I(t)}{I_\infty}$ versus time. I(t) is the Raman intensity of the LO peak after annealing during the time t. $I_\infty$ is the intensity of the same peak when saturation is reached. The slopes of the linear parts of the curve give the product $\alpha.v_g$. The recrystallization rate $v_g$ for the three values of temperature is given in Table 1.

TABLE 1. - Recrystallization velocity at different temperatures

| Temperature (°C) | 200 | 220 | 240 |
|---|---|---|---|
| $v_x$ (Å/min) | 4,9 | 13,9 | 24,2 |

Under the assumption that the temperature dependence of the recrystallization velocity is given by the relation :

$$v_x = v_o \exp (- E/kT)$$

the activation energy of this process can be evaluated as E = 1eV.

# 3. - LASER ANNEALING

## 3.1. Laser annealing of implanted silicon

### 3.1.1. Experimental conditions

For the investigation[4] of the recrystallization of amorphous materials by an intense laser beam, single crystal silicon samples are first amorphized by silicon ion implantation and then locally recrystallized over large areas of 0,4 to 1 mm diameter using isolated energetic single shot laser pulse. The crystalline quality of annealed regions is then tested by sweeping the recrystallized area with a much smaller Raman laser probe beam whose diameter is of the order of 80 μ.

Boron dopped, $\rho = 10^{-2}$ Ωcm, single crystal silicon (100) samples are subjected to $^{28}Si$ ion implantation under conditions such as to obtain amorphous layer of thickness 1500 Å or 5000 Å. Recrystallization is induced using a Q-switched ruby laser with 100 ns pulse duration giving a deposited energy density varying from 0,6 to 3.2 $J.cm^{-2}$.

### 3.1.2. Results and discussion

The amorphous to single crystal transition is detected by the appearance of the 520,5 $cm^{-1}$ Raman peak in the central region of the irradiated zone. Argon laser line of $\lambda = 4880$ Å being used in this experiment, the penetration depth at this wavelength is of the order of 10 000 Å in single crystal silicon and ten times less in amorphous material.

When a thick amorphous layer, W = 5000 Å, is laser annealed, as shown in Figure 8, where the large circle represents the area covered by the power laser and the dot the Raman probe beam, the Raman spectrum consists of a broad peak displaced from the normal mode frequencies of the perfect crystal $\omega_{LO}$, toward the lower frequencies. Far from the center of the annealed region the Raman peak is at

$\omega_d$ = 515 $cm^{-1}$ having a width $\Delta\omega_d$ = 10 $cm^{-1}$, whereas at the center of the spot $\omega_L$ = 510 $cm^{-1}$ and $\Delta\omega_L$ = 6 $cm^{-1}$. If the probing beam is just at the edge of the annealed region the spectrum consists simultaneously of the broad band due to amorphous material and the displaced $\omega_{LO}$ due to unperfectly recrystallized material. The frequency shift is account far by the effect of dimensions[5] of small crystallites formed in the intermediate region between amorphous and single crystal.

In Figure 9 are shown the spectra taken on a much thinner amorphous layer, W = 1500 Å. When the exploring Raman beam is now at the center of laser annealed spot the frequency of the Raman peak is exactly equal to the frequency of the normal mode of the perfect crystal $\omega_{LO}$ = 520,5 $cm^{-1}$. When the probing beam moves of the center of the spot two peaks are present in the Raman spectrum : the first corresponds to $\omega_{LO}$ and the second is at the displaced Raman frequency $\omega_d$. Moving from the center toward the periphery of the annealed spot the intensity of the peak due to $\omega_{LO}$ decreases and that of the shifted peaks $\omega_d$ increases. When the exploring spot approaches near the periphery of the annealed spot its frequency tends toward $\omega_d$ = 515 $cm^{-1}$ and its intensity dominates the spectrum. The center of the annealed region, when the initial amorphous layer is only 1500 Å tick, seems now perfectly well recrystallized. The crystalline structure of the peripheral region remains considerably perturbed. The shift in frequency is, we think, due to effect of dimensions and therefore the existence of the two peaks simultaneously due to a mixture of crystallites of different dimensions.

### 3.1.3. Effect of dimensions on the vibrational frequencies of thin slabs of silicon[5]

To understand the frequency shift in the amorphous to crystalline transition by laser annealing we were lead to the assumption that in think amorphous layers the recrystallization can not be an epitaxial grow. This transition proceeds rather through the formation of small crystallites whose dimensions depends on the vicinity of bulk amorphous material. To verify this assumption we have calculated the frequency shift of $\omega_{LO}$ due to the effect of dimensions.

The theoretical model used is very simple. We consider the case of a thin slab limited in one direction and extended to infinity in the two other directions. The slab is considered to consist of a number of layers, each of which has the thickness of a unit cell. In such a structure the periodicity of the lattice is conserved along the two directions, and, consquently the atomic displacements parallel to these conditions can be expanded in plane waves, and the periodic boundary conditions can be applied. Along the third direction neither of the above considerations is applicable, and the sequence of cells along that direction is treated merely as one unit cell. In order to reduce the dynamical matrix and avoid computational difficulties resulting from the increase of independent interactions due to the fact that we have to account for the interactions of layered lattices, the orientation of the slab is chosen to be across directions of high symmetry. For silicon the (111) plan is favourable for these calculations. For any slab having this orientation the solutions giving the vibrational mode frequencies are separated into two groups, one doubly degenerated containing the solutions corresponding to modes which vibrate in the two directions where the slab extends to infinity : xy modes, and one non degenerate containing the solutions corresponding to vibrations perpendicular to the surface of the slab, z modes.

The frequencies of the vibrational modes for slabs having thickness from 1 to 50 unit cells have been calculated.

The xy modes as well as the z modes are grouped in two regions separated by a large gap. All the modes of the upper group are of optical type, e.g. every pair of atoms in each cell moves in antiphase, while all the modes of the lower group are of accoustic type. The distribution of the "optical" xy modes shows two peaks near the limit of frequency interval in which they are contained, while the distribution of the z modes shows only a peak at the upper end of the range.

Weighted frequency distributions of xy and z optical modes with a weighting factor inversely proportional to the slab thickness are shown in Figure 10.

The frequency distribution of the 1 to 5 layers sum shows a pronounced maximum at 480 $cm^{-1}$ near the maximum of the absorption band of the Raman spectra. For the case of thicker slabs 11-15 and 21-25 unit cells thick the frequency distribution of optical modes shows two sharp peaks near the maximal frequency of vibrations $\omega_{LO}$ of the crystal. The low frequency mode progressively shifts toward the maximum frequency where the thickness is increased.

These features are exactly what has been observed in the Raman spectra of laser annealed ion implanted silicon in the intermediated recrysrallization stage. The experimental results are summarized in Figure 11. These spectra can be explained if a distribution of very small crystallites of different sizes is assumed. As the distribution of crystallites moves toward large sizes, the observed spectrum shifts from the one of the amorphous material to that exhibiting a second peak near the upper end, superimposed on the peak originating from the amorphous material spectrum but sharpened and shifted toward the high frequency region.

### 3.2. Laser annealing in ion implanted GaAs

The laser annealing of implanted GaAs is done with an YAG laser provided with a frequency doubler delivering simultaneously the two wavelength 1.06 and 0.53 μ with a total energy density less than 0.8 $J/cm^2$. Higher energy density destroys the samples. If only the wavelength of 1.06 μ is used the recrystallization of the material is not easy. The adsorption edge of GaAs is at 0.9 μ, light at 0.53 μ is adsorbed in a very thin superficial layer creating an dense electron hole plasma. The beam of 1.06 μ is then absorbed in the free electron gaz and the energy transfered consequently to the lattice

In Figure 12 we represent results obtained in exploring the (100) face of GaAs made amorphous by As implantation with a dose of $10^{14}$ ions/$cm^2$. The annealing is done at an energy density of 0.6 $J/cm^2$ with a spot having a diameter of 6 mm. The analysis is performed with an incident Raman laser beam whose width is of the order of 80 μ.

When the exploring Raman beam is focussed outside the annealed region the spectrum obtained is that of amorphous GaAs. When the analyzing beam is focussed at the edge of the annealed and the amorphous regions the spectrum shows a band in the vicinity of the TO mode frequency. As the exploring beam is moved toward the center of the annealed region the band sharpens and its frequency shifts toward the TO mode frequency of the perfect crystal, a shoulder appears which also sharpens as the Raman spot moves toward the center, its frequency progressively increases and approaches the LO mode frequency of the GaAs lattice. At the center of the annealed region where one may suppose that perfect crystal GaAs is obtained the Raman scattered intensity of the two peaks is inversed : the LO peak becomes far more intense than the TO peak.

The TO peak is normally forbiden for the (100) face of GaAs and yet it is observed even with higher intensity than the allowed LO peak in the intermediate region. The activation of the forbiden TO peak is probably due to an imperfect recrystallization of GaAs : at the peripherical region microcrystallites are formed misaligned with respect to the substrate orientation and consequently the selection rules are violated and TO observed giving evidence for the existance of misoriented crystallites. The recrystallization at this annealing beam energy remains imperfect even at the center of the annealed region : the LO and TO mode frequencies remain always lower than the normal modes frequency of the perfect GaAs lattice.

In Figure 13 we show the analysis in polarized light. The incident electric field vector is along the (011) axes ; the scattered electric field vector is analyzed in two directions : parallel to (011) or perpendicular to (011). The TO mode is normally forbiden ; the LO mode is allowed when the incident and scattered electric field vectors are parallel and extinguished when they are perpendicular. If the microcrystals are large enough we observe exactly the predictions of the selection rules, e.g. at the center of the annealed region where the recrystallization is almost achieved. In the peripheral region the evolution of the light scattering spectra is continuous between the amorphous behaviour and the misaligned polycrystalline region.

## 4. - CONCLUSION

It has been clearly shown in this investigation that light scattering spectroscopy is a powerful tool for studying the amorphous crystalline transition.

The thermal annealing is always done at temperatures such that it is impossible to think of a melting of the lattice and eventual epitaxial grow as mechanism for recrystallization of amorphous material. On the basis of the experimental results presented here one is rather lead to envisage atomic diffusion in the amorphous material with an activation energy toward positions favourable to the nucleation and grow of small crystallites. With thermal annealing for sufficiently long times the crystallites merges into a large single crystal and the structure of normal mode of vibrations is recovered in the Raman spectrum.

Detailed results of particular interest have been obtained in the case of laser annealing. It becomes now clear that laser annealing do not proceeds through fusion and epitaxial growth as many authors have previously supposed. A rather more plausible model [6] seems to be that imploying the creation of a dense electron hole plasma by the power laser beam. At the periphery of the area irradiated by the laser some of the electron hole pairs may diffuse out of the dense region subject to concentration gradient. Inside the dense region the electron hole pairs may condense into electron hole droplets. The exchange of energy with the lattice at the sites where droplets are formed, favorizes the atomic displacements in the amorphous material toward positions favourable to nucleation and subsequent grow of microcrystallites. The density of droplets being maximum in the center of the irradiated area the nucleation density is high and leads to the formation of a single crystal of large sizes in which the normal mode of vibration of the perfect lattice is observed. Toward the periphery the concentration of droplets is smaller, the nucleation sites are spread and isolated small crystallites are formed. This is

clearly shown with Raman spectroscopy : in the intermediate region between amorphous and crystalline material the size of the crystallites is progressively growing toward the center and the characteristic Raman peak shifting from a distribution identifying the amorphous material to that of a polycrystalline region. The size of micro-crystallites is also progressively increasing when going from the periphery toward the center of the annealed region as shown by the correspondance of the Raman data and lattice dynamics calculations taking into account the effect of dimensions.

ACKNOWLEDGMENTS

This research was supported in part by the European Research Office of the U.S. Army Grant N° DA-78-G-002.

## REFERENCES


(1) J.F. MORHANGE, R. BESERMAN, M. BALKANSKI,
Phys. Stat. Sol. (a) 23, 383 (1974).

(2) R.L. FARROW, R.K. CHANG, S. MROCZKOWSKI, F.H. POLLACK,
Appl. Phys. Lett. 31, 768 (1977).

(3) J.W. MAYER, L. ERIKSON, S.T. PICRAUX, J.A. DAVIES,
Can. J. Phys. 46, 663 (1968).

(4) J.F. MORHANGE, G. KANELLIS, M. BALKANSKI,
Sol. Stat. Comm., 31, 805 (1979).

(5) G. KANELLIS, J.F. MORHANGE, M. BALKANSKI,
Phys. Rev. B21, 1543 (1980).

(6) J.A. VANVECHTEN, R. TSU, F.W. SARIS,
Phys. Lett. 74A, 422 (1979).

## FIGURES CAPTIONS

Figure 1. Raman spectra of Silicon rendered amorphous by $10^{16}$ ions As/cm$^2$.

Figure 2. Isochronal annealing behaviour of silicon implanted with $10^{16}$ ions As/cm$^2$.

Figure 3. Isothermal annealing behaviour of Silicon implanted with $10^{16}$ ions As/cm$^2$.

Figure 4. Raman spectra of crystalline and amorphous Gallium Arsenide.

Figure 5. Isochronal annealing behaviour of Gallium Arsenide implanted with $10^{15}$ ions P/cm$^2$.

Figure 6. Scattering geometry during isothermal annealing.

Figure 7. Variation of the LO phonon intensity during isothermal annealing.

Figure 8. Raman spectra for various positions of the probing laser along the diameter of a laser annealed region. The Silicon amorphous depth layer is 500 nm.

Figure 9. Raman spectra for various positions of the probing laser along the diameter of a laser annealed region. The Silicon amorphous depth layer is 150 nm.

Figure 10. Weighted distribution of the optical modes of a thin slab.

Figure 11. Raman spectra from points at the periphery of a laser annealed Silicon.

Figure 12. Raman spectra for various points of a laser annealed region in Gallium Arsenide.

Figure 13. Polarization measurement of a laser annealed region in a Gallium Arsenide sample.

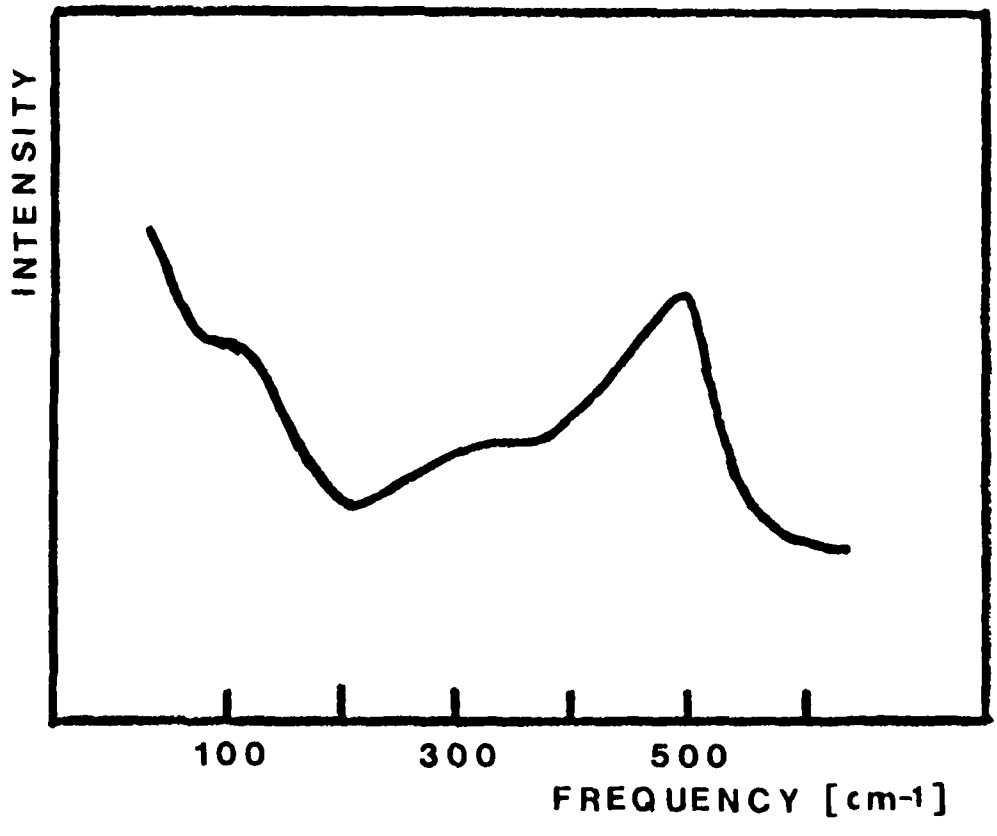
INTENSITY
100
300
500
FREQUENCY [cm-1]

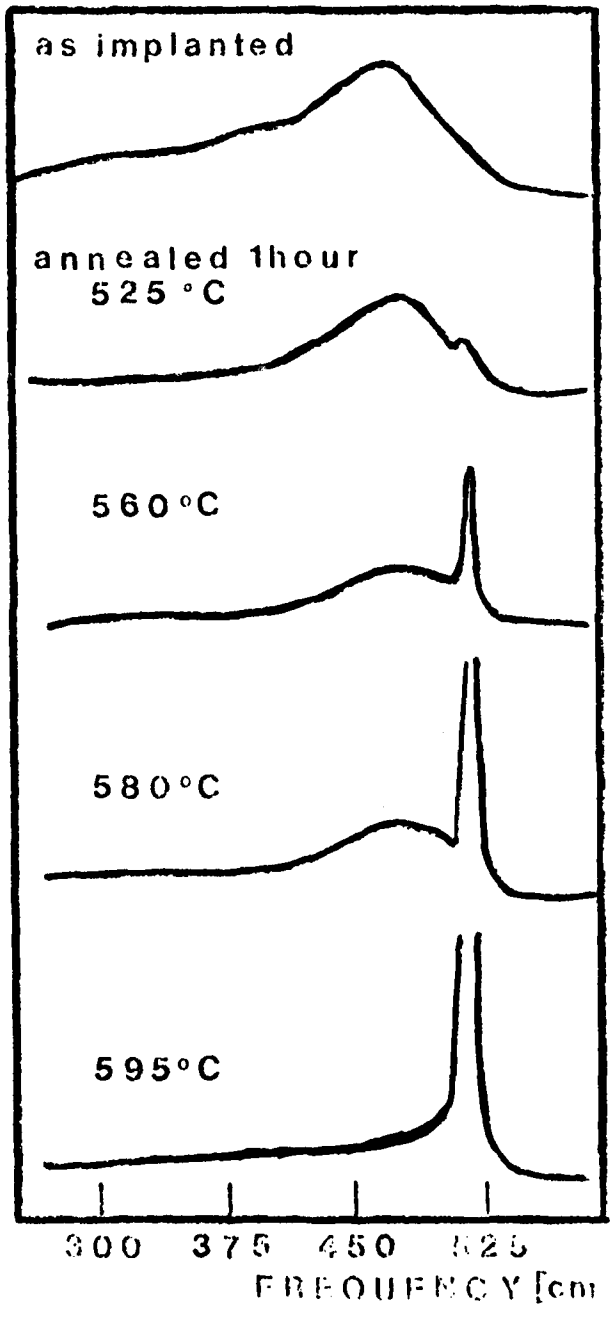
as implanted
annealed 1hour
525 °C
560°C
580°C
595°C
300
375
450
525
FREQUENCY [cm-1]

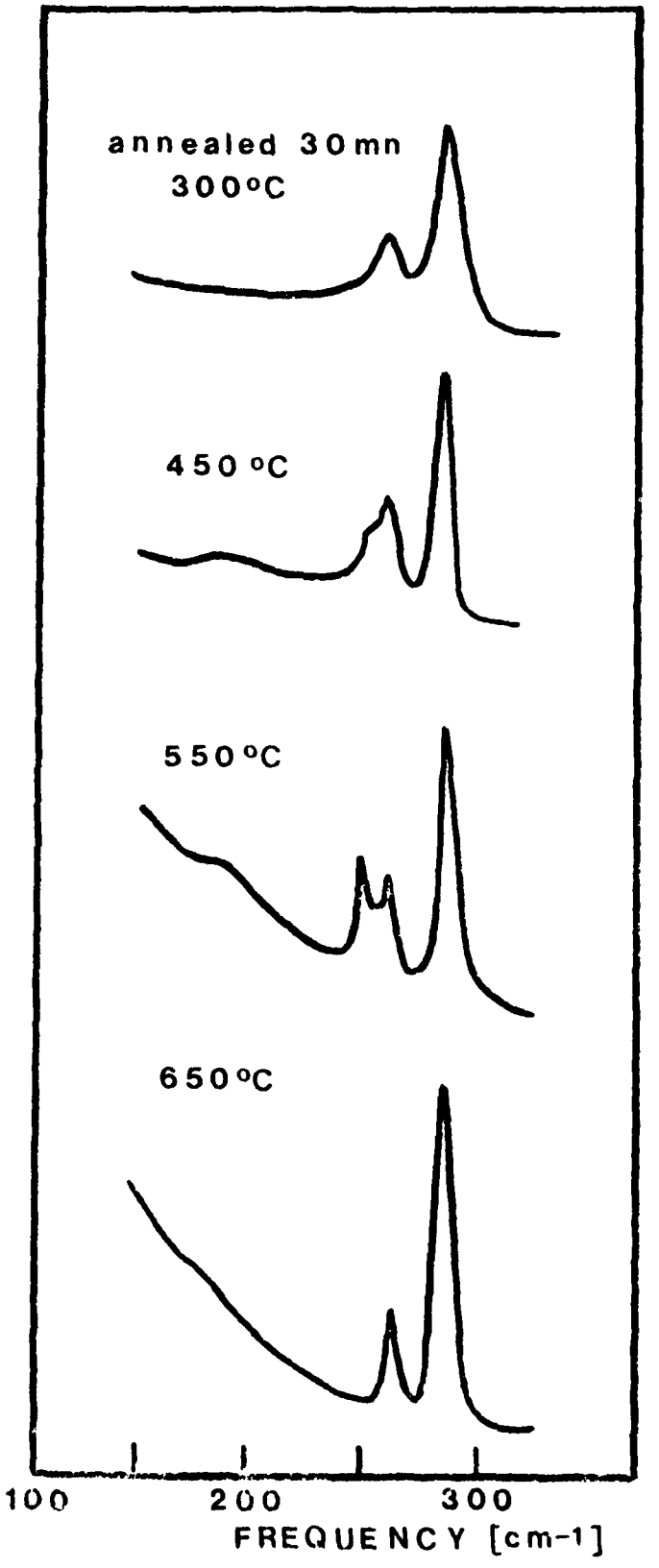
annealed 30mn
300°C
450 °C
550°C
650°C
100
200
300
FREQUENCY [cm-1]

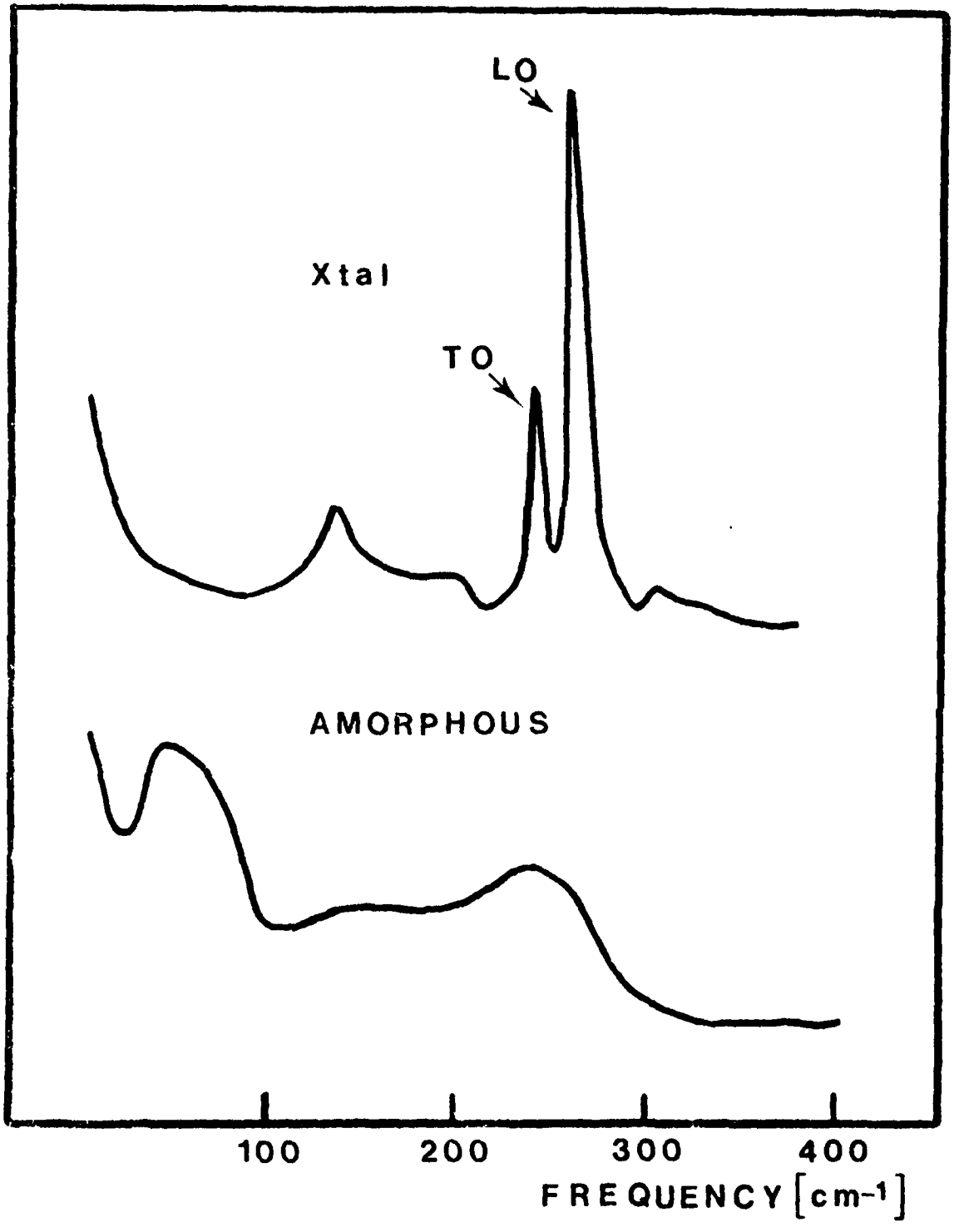
LO
Xtal
TO
AMORPHOUS
100
200
300
400
FREQUENCY [cm-1]

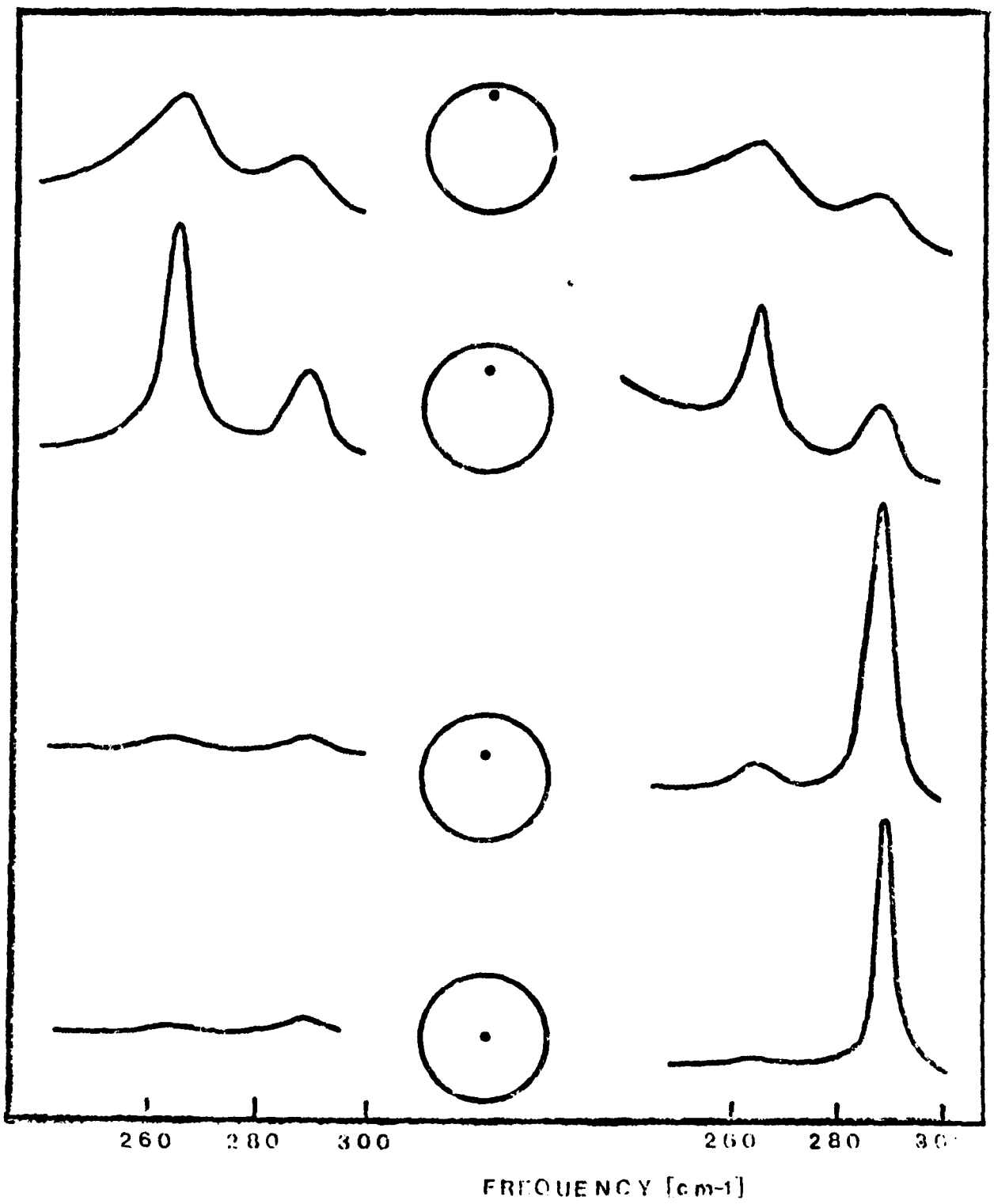
260
280
300
260
280
FREQUENCY [cm-1]

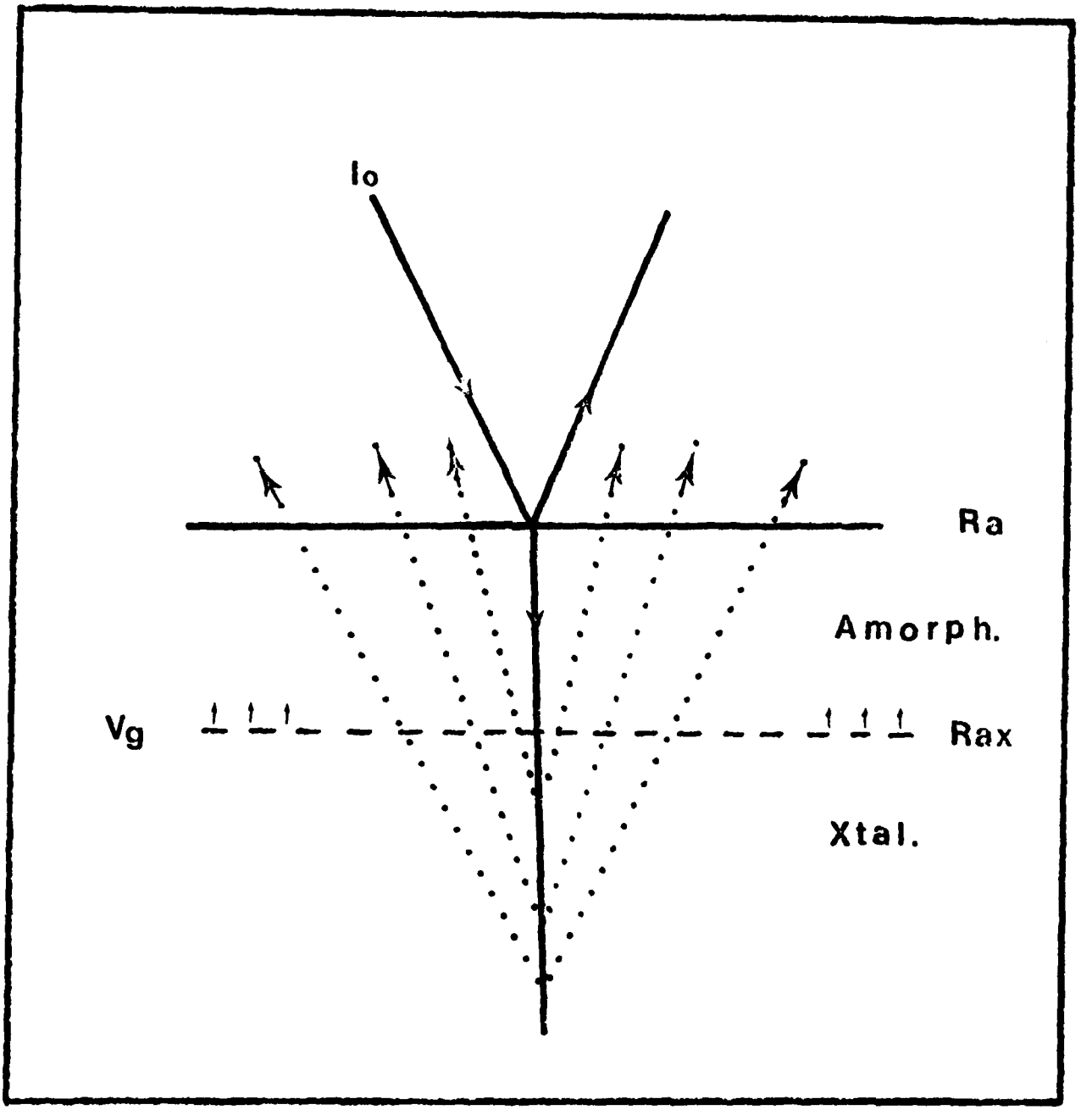
Io
Ra
Amorph.
Vg
Rax
Xtal.

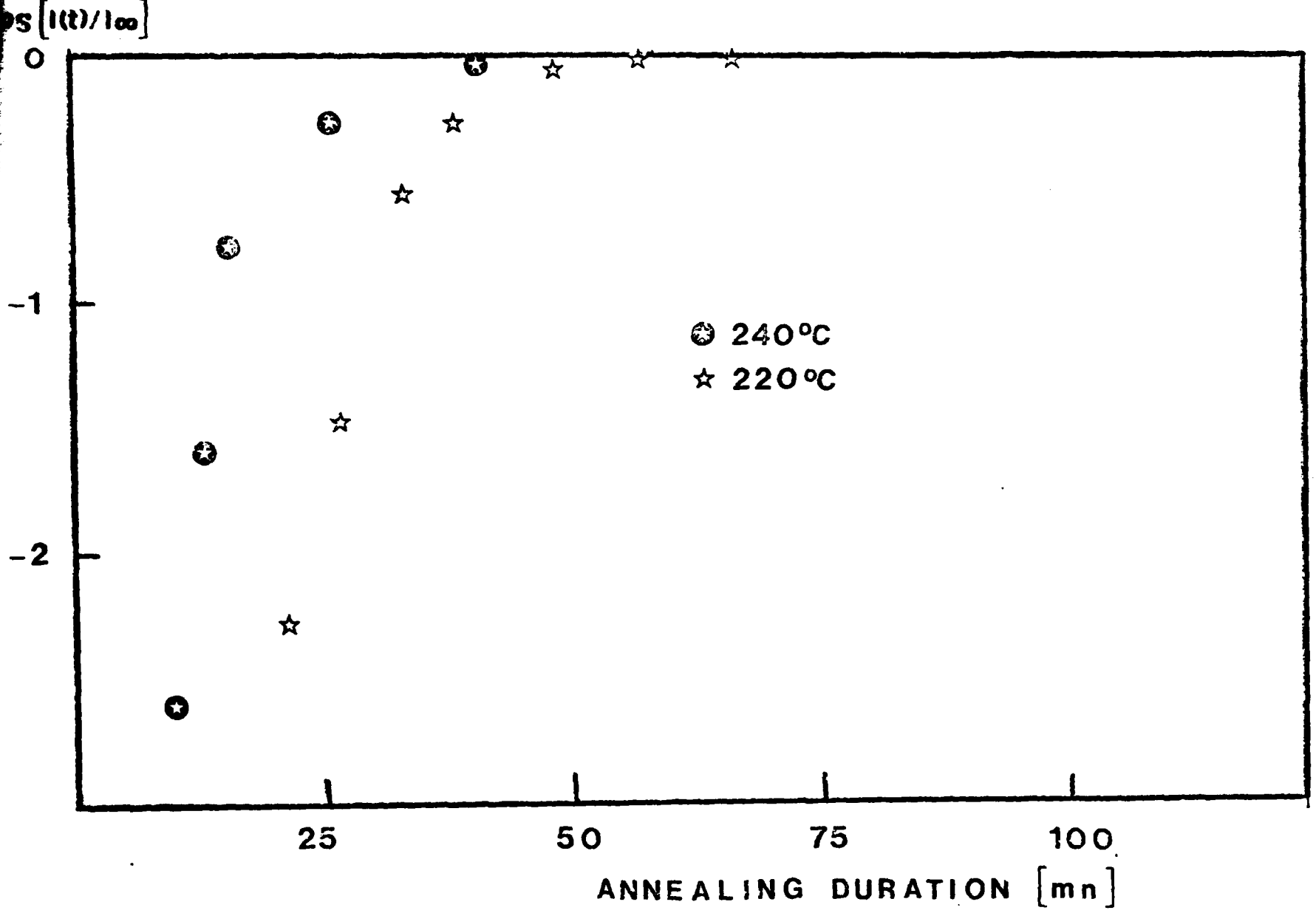
Ln [I(t)/I∞]
0
-1
-2
240°C
220°C
25
50
75
100
ANNEALING DURATION [mn]

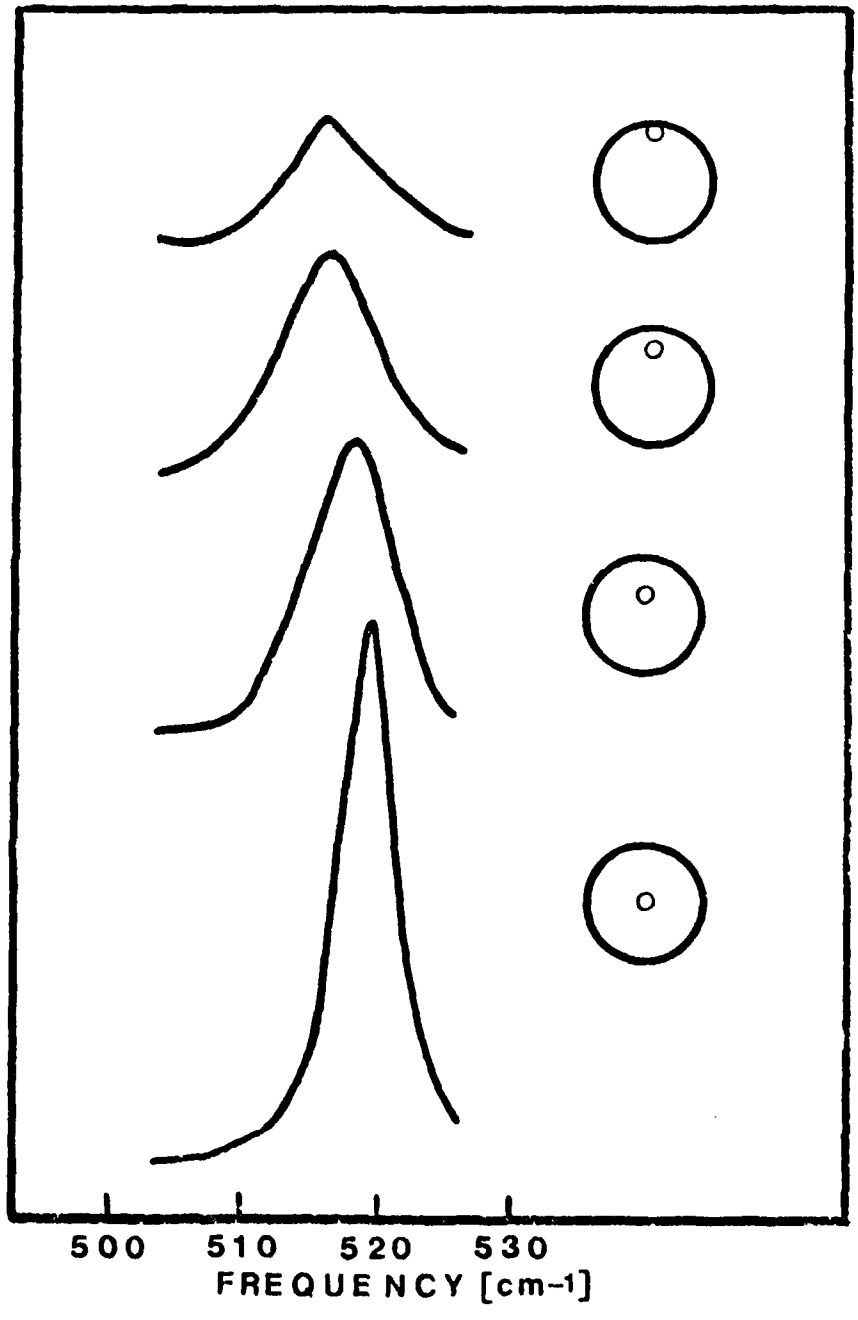
500
510
520
530
FREQUENCY [cm-1]

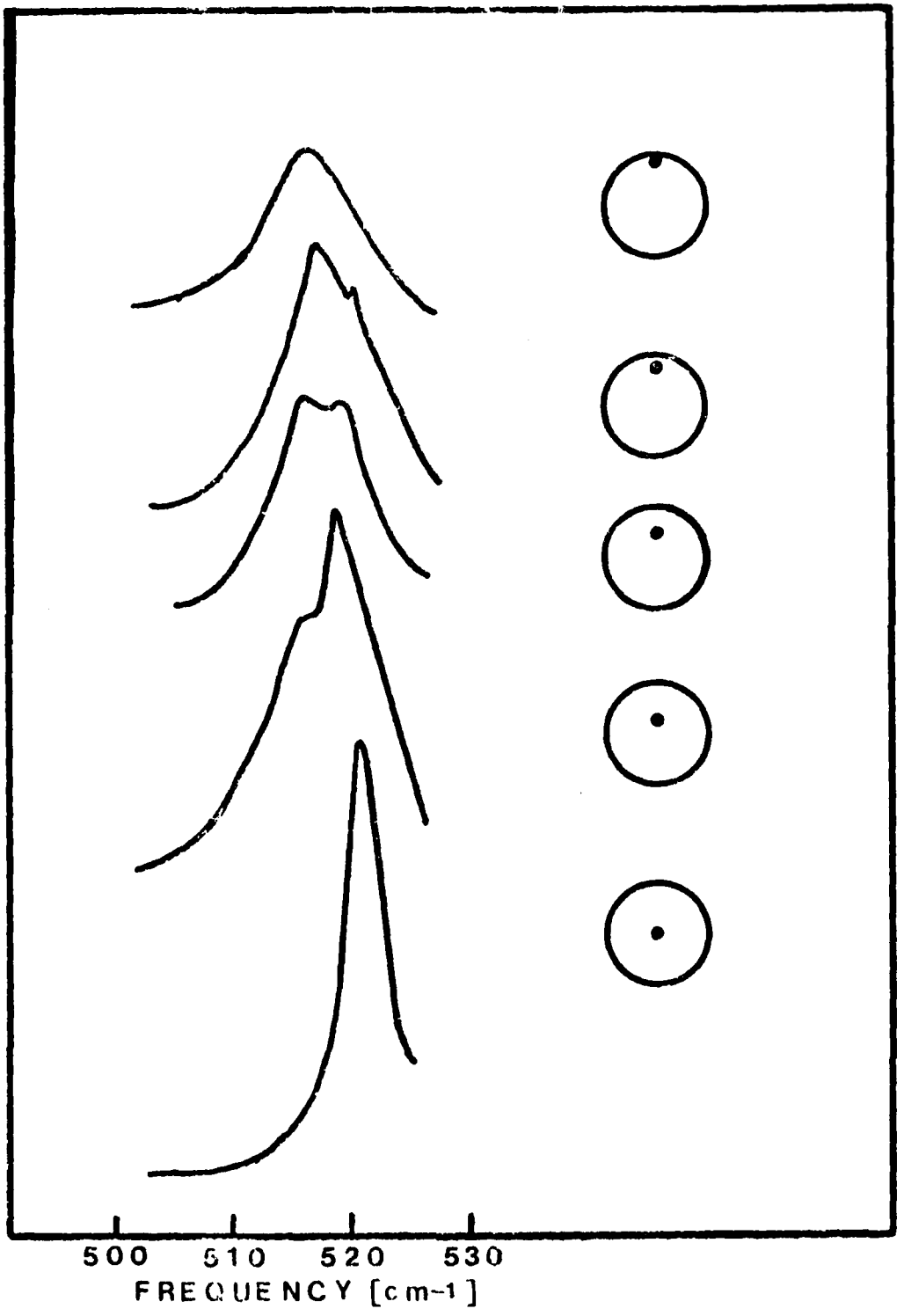
500
510
520
530
FREQUENCY [cm-1]

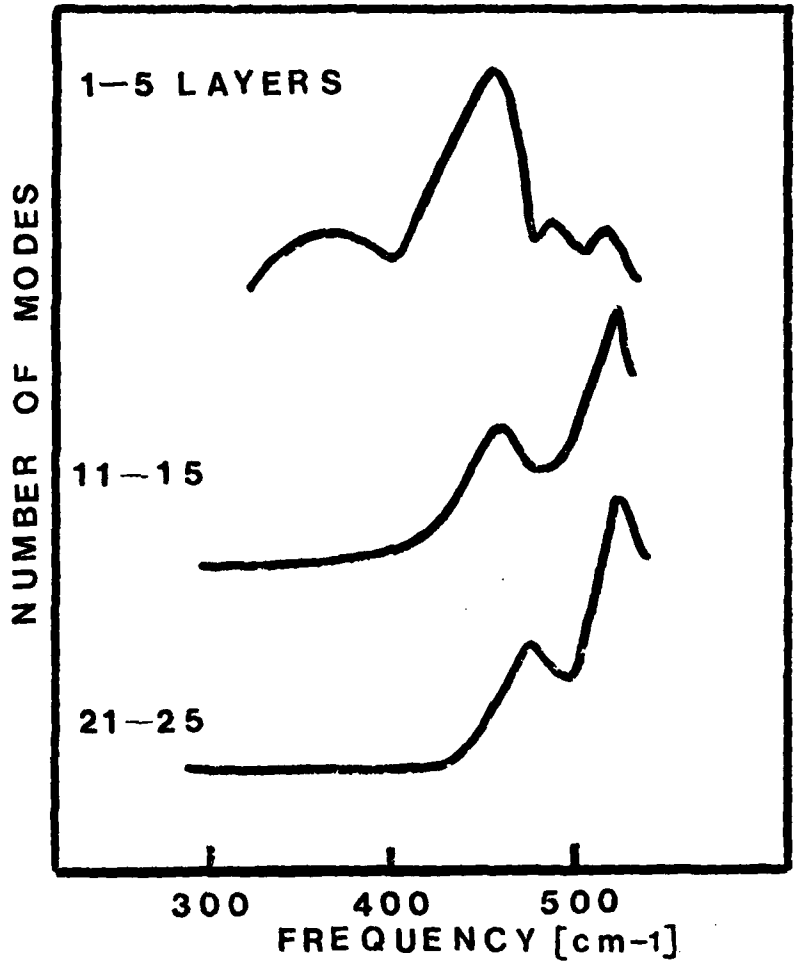
1—5 LAYERS
11—15
21—25
NUMBER OF MODES
300
400
500
FREQUENCY [cm-1]

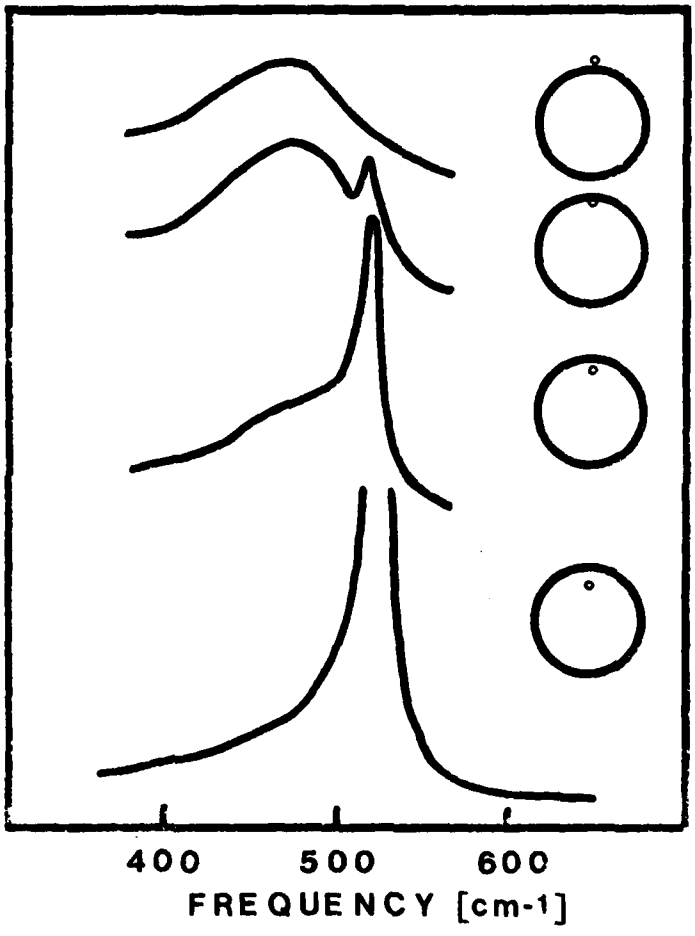
400
500
600
FREQUENCY [cm-1]

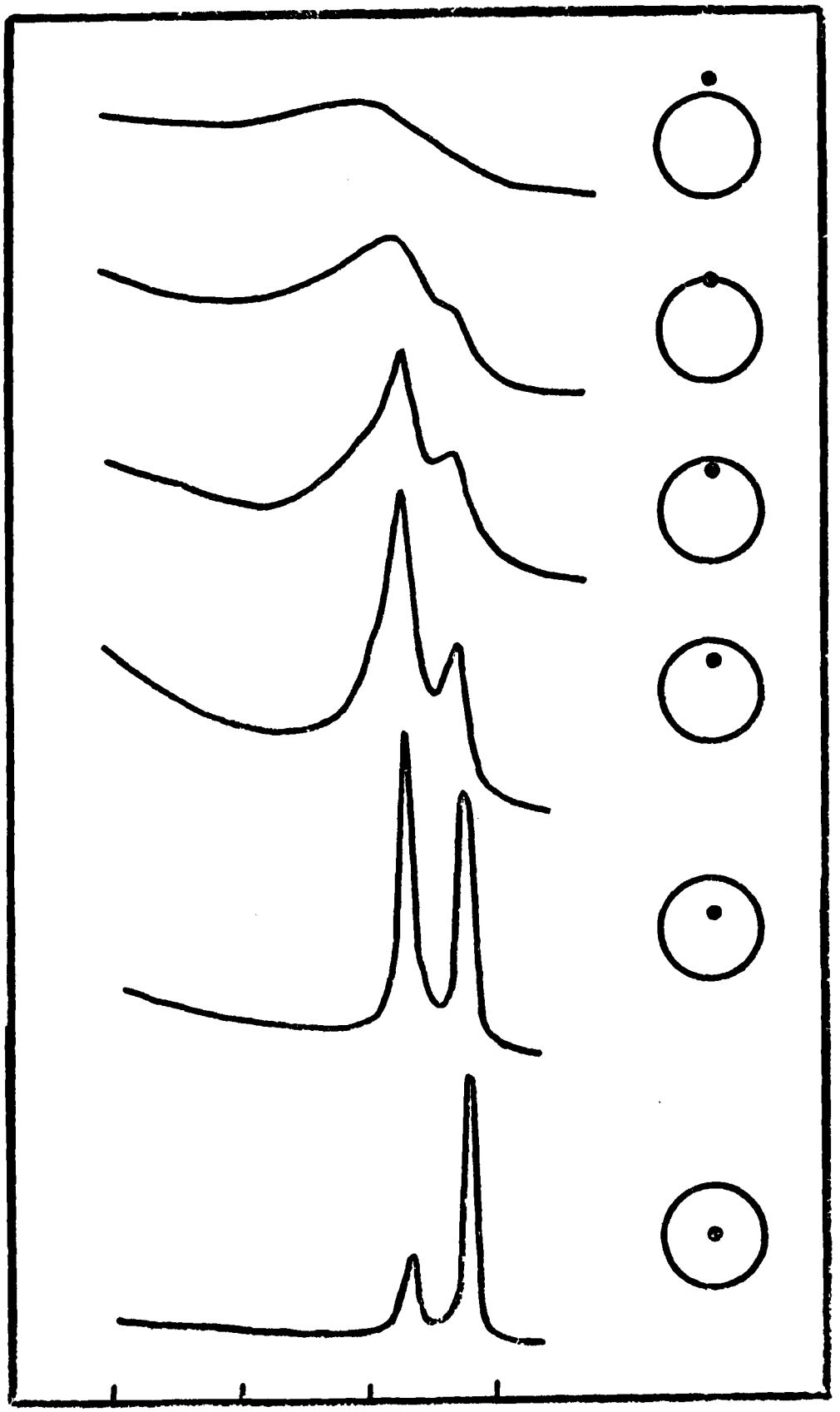
150
200
250
300
FREQUENCY [cm⁻¹]

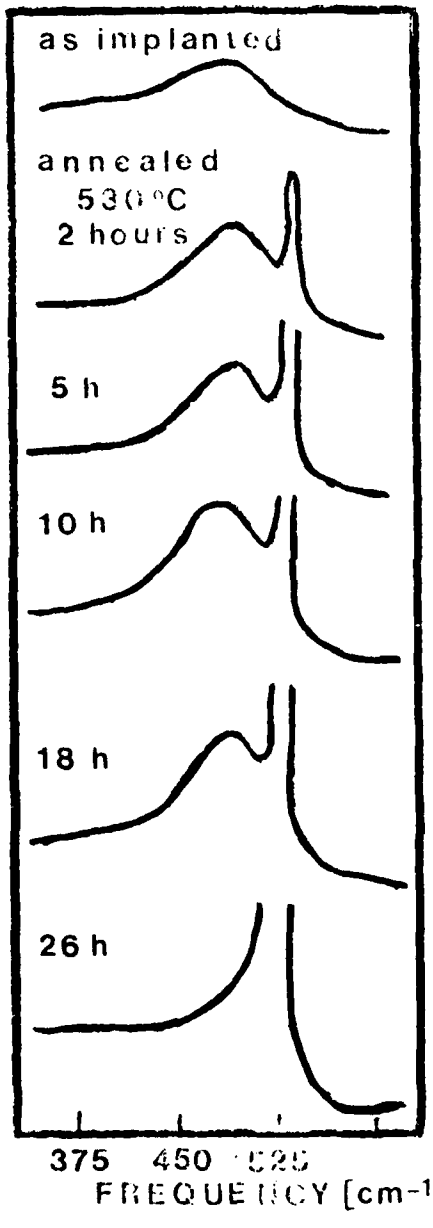
as implanted
annealed
530°C
2 hours
5 h
10 h
18 h
26 h
375
450
525
FREQUENCY [cm-1]